HHS Public Access

Author manuscript

Nat Microbiol. Author manuscript; available in PMC 2020 June 09.

Published in final edited form as:

Nat Microbiol. 2020 January ; 5(1): 206–215. doi:10.1038/s41564-019-0610-7.

Regulation underlying hierarchical and simultaneous utilization of carbon substrates by flux sensors in *Escherichia coli*

Hiroyuki Okano[1,†,*], **Rutger Hermsen**[2,†,*], **Karl Kochanowski**[3,4,#], **Terence Hwa**[1]

[1]Department of Physics, University of California at San Diego, La Jolla, CA 92093-0374 [2]Theoretical Biology and Bioinformatics Group, Department of Biology, Faculty of Science, Utrecht University, Padualaan 8, 3584 CH Utrecht, The Netherlands [3]Institute of Molecular Systems Biology, ETH Zurich, Zurich, Switzerland [4]Life Science Zurich PhD Program on Systems Biology, Zurich, Switzerland.

Abstract

Many microbes exhibit nutrient preferences, exemplified by the “hierarchical” consumption of certain carbon substrates. Here we systematically investigate under which physiological conditions hierarchical substrate utilization occurs and its mechanisms of implementation. We show utilization hierarchy of *Escherichia coli* to be ordered by the carbon-uptake flux rather than the identity of the substrates. A detailed study of glycerol uptake finds that it is fully suppressed if the uptake flux of another glycolytic substrate exceeds a threshold, set to the influx obtained when grown on glycerol alone. Below this threshold, limited glycerol uptake is “supplemented” such that the total carbon uptake is maintained at the threshold. This behavior results from total-flux feedback mediated by cAMP-Crp signaling, but also requires inhibition by regulator fructose-1,6-bisphosphate, which senses the upper *glycolytic* flux and ensures that glycerol uptake defers to other glycolytic substrates but not to gluconeogenic ones. A quantitative model reproduces all observed utilization patterns including those of key mutants. The proposed mechanism relies on differential regulation of uptake enzymes and requires a specific operon organization. This organization is found conserved across related species for several uptake systems, suggesting the deployment of similar mechanisms for hierarchical substrate utilization by a spectrum of microbes.

[*]Correspondence and material requests should be addressed to Hiroyuki Okano, okanoh@physics.ucsd.edu and to Rutger Hermsen, r.hermsen@uu.nl.

[†]These authors contributed equally to this work.

[#]Present address: Karl Kochanowski, Department of Pharmaceutical Chemistry, University of California at San Francisco, San Francisco, CA 94158-2330

AUTHOR CONTRIBUTIONS

HO and TH designed the experiments. HO performed most of the experiments. KK performed mass spectrometric experiment and analysis. RH performed the quantitative modeling and theoretical analysis. HO, RH, and TH analyzed the data and wrote the paper.

COMPETING INTEREST STATEMENT

The authors declare that the authors have no competing interests as defined by Nature Research, or other interests that might be perceived to influence the results and/or discussion reported in this paper.

INTRODUCTION

Bacteria grown on multiple carbon substrates often consume them sequentially, using some only after others are depleted[1,2]. This “hierarchical” order of utilization has been studied most intensely in *E. coli*[1,3–5], particularly through the iconic diauxic growth on lactose and glucose[6,7]. However, several studies have demonstrated that mixtures of carbon substrates that are utilized hierarchically in batch cultures are utilized simultaneously in carbon-limited chemostat cultures[8–10]. Likewise, if multiple substrates are present at low concentrations, they are often utilized simultaneously even in batch culture[8,11–13]. Intriguingly, hierarchical utilization appears to be limited to combinations of glycolytic substrates: gluconeogenic substrates tend to be co-utilized with other substrates[14]. Together, these observations raise questions regarding the strategies and mechanisms bacteria use to control their carbon utilization.

In this work, we address these questions for several exemplary substrate pairs in *E. coli*. After showing similar physiological behavior on a variety of substrate pairs, we focus on glycerol uptake in the presence of glycolytic substrates glucose or lactose. As shown in Fig. 1a,b and Extended Data 1, the utilization of these substrate pairs is hierarchical: glycerol is not consumed until glucose or lactose is depleted. Through quantitative characterization, we establish that glycerol uptake responds to the total carbon-uptake flux, including glycerol uptake itself. Glycerol uptake is turned off if this total carbon-uptake flux exceeds a threshold set slightly above that on glycerol alone. If the total flux is below that threshold, glycerol is co-utilized with the other substrates, but only such that the total flux is maintained at approximately the same level as that on glycerol alone. This flux-based regulation dictates that glycerol is *simultaneously* utilized with other substrates when their flux is sufficiently low, explaining why simultaneous utilization is rather general for mixtures of substrates present at low concentrations, including continuous cultures.

We also address how this flux-based regulation of glycerol uptake is implemented molecularly, using a computational model based on known regulatory interactions[15,16]. We demonstrate that the response of glycerol uptake to other substrates is implemented by feedback loops mediated by cAMP–Crp, reflecting the total carbon-uptake flux, and fructose-1,6-bisphosphate (FBP), reflecting the upper-glycolytic flux. The latter elucidates how the cell distinguishes glycolytic from gluconeogenic substrates and accordingly switches between hierarchical and simultaneous utilization.

We also show that implementation of the total-flux feedback is facilitated by the chromosomal organization of the glycerol degradation pathway in two separate operons. Strikingly, this organization is found for many other degradation pathways and conserved in related species, suggesting that total-flux feedback is employed for hierarchical substrate utilization by a spectrum of microbes.

RESULTS

Patterns of hierarchical and simultaneous utilization

Titratable uptake of the preferred substrate—Since its discovery, diauxic growth has been the primary way to study hierarchy in carbon-substrate utilization[1]. However, to elucidate the mechanisms involved, it is necessary to study the regime where the preferred substrate is running out and the cell begins to metabolize the second substrate. The transient nature of this "diauxic shift" makes a quantitative characterization difficult to perform. Here, we exploit strains that allow the cellular response to the depletion of the preferred substrate to be studied in batch cultures under balanced exponential growth. Because maintaining fixed low substrate concentrations during exponential growth is difficult, we use *E. coli* strains in which the expression of a substrate uptake system—and hence that substrate's uptake flux—can be controlled by varying the concentration of an inducer (3-methylbenzyl alcohol, or 3MBA) in the growth medium (Fig. 1c)[16]. Thus, we mimicked the reduced uptake flux of the preferred substrate when it runs out while keeping its actual concentration at saturating levels. We employed three such strains (NQ917, NQ1243, NQ399; see Supplementary Figure 1), in which the expression of LacY, PtsG, and GlpF/GlpK, the uptake systems for lactose, glucose, and glycerol, can be finely titrated.

A tight growth-rate crossover—We first studied the growth of the titratable LacY strain (NQ917), using minimal medium with glycerol, lactose, or both, at various concentrations of 3MBA (Fig. 2a). At low 3MBA concentrations (low LacY expression), the growth rate on the two substrates (pink circles) was similar to that on glycerol only (orange triangles), while at high 3MBA concentrations (high LacY expression) it was similar to that on lactose only (green diamonds). A tight crossover between these regimes occurred at [3MBA] ≈ 100 μM and a growth rate of 0.7—0.8/h, near the intersection of the pink circles and the orange triangles (indicated with a red arrow). Remarkably, the growth rate never dipped below that on glycerol only (≈ 0.7/h). A very similar behavior was found using the titratable PtsG strain (NQ1243) with glucose instead of lactose (Fig. 2b) and, importantly, for many other substrate combinations (see Extended Data 2).

A threshold separates hierarchical and simultaneous utilization—To elucidate the growth-rate crossovers, we measured the uptake of glycerol and lactose (in the presence of both) at various 3MBA levels (Fig. 2c). For lactose uptake above a threshold (dashed horizontal line at $j_{th} \approx 25$ ℂ, where ℂ =1 mM of carbon atoms per OD_{600} per hour), no glycerol was taken up. But when it fell below the threshold, the cells *supplemented* it with glycerol. The threshold occurred at [3MBA] ≈ 100 μM (vertical dashed line), corresponding to the occurrence of the growth-rate crossovers shown in Fig. 2a,b. Using single-cell measurements, we ruled out that this supplementation effect arises from population heterogeneity (Supplementary Figure 2).

Strikingly, throughout the supplementation regime glycerol uptake adapted such that the *total* carbon-uptake flux (Fig. 2c) remained approximately *constant* despite a three-fold change in lactose uptake, at a level corresponding to that of growth on glycerol alone, (23 ± 1)ℂ (error represents 95% CI, $n = 11$ independent measurements). The same pattern was

found for the titratable PtsG strain (NQ1243), with a remarkably similar threshold value $j_{th} \approx 25$ ℂ (Fig. 2d). Because glycerol and glucose are co-utilized in the supplementation regime, the diauxic lag vanishes there (see Extended Data 3).

A threshold-linear flux relation as a hallmark of hierarchical utilization—If glycerol uptake is plotted against lactose uptake (Fig. 2e) or glucose uptake (Fig. 2f), a nearly threshold-linear relation is seen. This "flux relation" reveals the transition from a supplementation regime (a straight line with a slope of approximately −1) to a hierarchical regime (no glycerol uptake) if the uptake of the preferred substrate exceeds the threshold $j_{th} \approx 25$ ℂ. This flux relation is more revealing than the diauxic lag, which is exhibited only under carefully chosen conditions (Fig. 1a,b, Extended Data 1, Supplementary Figure 3).

Regulation of glycerol uptake

To elucidate the features of hierarchical utilization described in Fig. 2, we turn to the regulation of glycerol uptake. The catabolism of glycerol has been studied in detail[15] (Fig. 3a and Supplementary Figure 4). The assimilation of glycerol into glycolysis requires two reactions, catalyzed by kinase GlpK and dehydrogenase GlpD, which are both transcriptionally repressed by specific repressor GlpR[17,18] and activated by cAMP–Crp. Repression by GlpR is relieved by inducer sn-glycerol-3-phosphate (G3P), which is the product of GlpK and the substrate of GlpD. GlpK is allosterically inhibited by fructose-1,6-bisphosphate (FBP), an intermediate of glycolysis[19]. (The PTS enzyme $EIIA^{Glc}$ is also known to inhibit GlpK allosterically, but this interaction has little or no effect on glycerol uptake during glucose-glycerol diauxie[20]; data presented below support this.)

Onset of glycerol uptake is due to GlpR derepression upon abrupt increase of its inducer G3P—To establish whether the abrupt onset in glycerol uptake at the threshold (Fig. 2c,d) is tied to the expression of the GlpK and GlpD enzymes, we measured LacZ reporter expression from the *glpFK* (strain HE305) and *glpD* (strain HE397) promoters in titratable PtsG strains. During growth on glucose + glycerol with various 3MBA concentrations, the LacZ expression from both promoters sharply increased when the 3MBA concentration was reduced below the threshold of 100 μM (Fig. 3b,c, purple squares). The abrupt onset of expression resulted from the relief of repression by GlpR, because in *ΔglpR* mutant strains (HE308 and HE398) this behavior is abolished (Fig. 3b,c, light-blue diamonds). Consistent with this, the flux relation of the *ΔglpR* strain (NQ958) shows a more gradual transition to glycerol consumption (Fig. 3d, light-blue diamonds).

The relief of repression by GlpR is due to an abrupt rise of the inducer G3P, as determined by mass spectrometry (see Materials & Methods): in the titratable LacY strain (NQ917) grown on lactose + glycerol, the G3P pool increased abruptly when the 3MBA level was reduced below the threshold of 100 μM (Fig. 3e, pink circles).

The tight coupling between onset of glycerol uptake and the relief of GlpR-dependent repression suggests that the lactose/glucose flux inhibits glycerol uptake by affecting the G3P pool. We therefore asked whether the remaining regulators, FBP and cAMP–Crp, could transmit information on the lactose/glucose flux to the G3P pool.

FBP senses upper-glycolytic flux and directly inhibits glycerol uptake—A recent study reported that the intracellular FBP pool increases linearly with the glycolytic flux and hence called FBP a glycolytic *flux sensor*[21]. To verify this, we measured the intracellular FBP pool in the titratable LacY strain (NQ917) grown on lactose alone and on lactose + glycerol, with various 3MBA concentrations. Across conditions, the FBP pool increased consistently with the lactose uptake flux (Fig. 4a) but not with the *total* glycolytic flux (including the glycerol flux) (Fig. 4b). This indicates that the FBP pool is sensitive to the flux through *upper* glycolysis (*i.e.*, to substrates entering glycolysis upstream of FBP) rather than to the total glycolytic flux (including substrates entering downstream). Since FBP is known to inhibit GlpK activity[19] (Fig. 3a and Supplementary Figure 4) and hence the synthesis of G3P, it can transmit information about the upper-glycolytic flux to the G3P pool.

cAMP–Crp senses the total carbon-uptake flux and sharply affects the G3P pool—Recent studies reported that, under variation of carbon sources and uptake rates, transcriptional activation by cAMP–Crp is a decreasing function of the growth rate; in particular, the expression levels of many catabolic genes regulated by cAMP-Crp decrease linearly with the growth rate[14,16,22]. We verified that this linear relation (called the "C-line"[16]) also applies under the growth conditions of this study (Fig. 4c). Because the growth rate correlates strongly with the total carbon-uptake rate (Supplementary Figure 5a,b), this also implies that cAMP–Crp can be considered a sensor of the total carbon-uptake flux.

cAMP–Crp activates the transcription of the two operons containing the glycerol degradation pathway (Supplementary Figure 4). To test whether cAMP–Crp signaling also affects the intracellular G3P pool, we studied a titratable LacY strain carrying *ΔglpR glpK22* double mutations. In this strain, the *glpK22* mutation renders GlpK insensitive to allosteric inhibition by $EIIA^{Glc}$ and FBP [19,23], and the *glpR* deletion removes specific repression by GlpR, so that GlpK and GlpD activity is controlled by cAMP–Crp only (Fig. 3a and Supplementary Figure 4). When this strain was grown on lactose + glycerol with various 3MBA concentrations, the intracellular G3P pool responded sharply to changes in the growth rate (Fig. 4d, purple squares), demonstrating that cAMP–Crp signaling affected the G3P pool. Such an increase was not observed for growth on lactose alone (Fig. 4d, green squares), ruling out effects due to conversion of other internal metabolites to G3P. The response differed markedly from that of the $glpR^+$ $glpK^+$ strain, where the G3P pool fell to the basal level as soon as the growth rate exceeded the threshold of 0.7/h (Fig. 3e). This confirms again that GlpR and/or allosteric inhibition by FBP are necessary for strict inhibition at the threshold.

Because the synthesis and turnover of G3P are dictated by GlpK and GlpD, the G3P level is affected by the ratio of GlpK to GlpD. Since their genes *glpK* and *glpD* reside in different operons, the effect of cAMP–Crp signaling on the G3P pool could be due to a difference in its effect on the expression of these operons (Extended Data 4). Indeed, in the *ΔglpR* and *ΔglpR glpK22* strains, in which *glpD* and *glpK* expression are controlled by cAMP–Crp only, reporter expression from the *glpK* promoter follows a C-line whereas reporter expression from the *glpD* promoter does not (compare light-blue diamonds in Fig. 3b and c). This demonstrates that *differential regulation* of the two operons by cAMP–Crp affects the

ratio of GlpK and GlpD expression and thus transmits information on the total carbon uptake to the G3P pool, hence affecting glycerol uptake.

Analysis and quantitative molecular model

The total-flux feedback strategy—Above, we observed that glycerol uptake (i) responds nearly identically to lactose and glucose uptake, (ii) is completely inhibited if lactose or glucose flux exceed a threshold j_{th}, and (iii) is *supplemented* if lactose or glucose flux is below j_{th}, such that total carbon-uptake flux is approximately constant and the growth rate is near the growth rate on glycerol alone.

In theory, observations (i)—(iii) can be implemented by a simple scheme that we call the *total-flux feedback strategy* (Extended Data 5). It is characterized by a single negative feedback loop: glycerol uptake is inhibited by a signal that represents the total carbon-uptake flux including glycerol uptake itself. Observations (i)—(iii) are attained generically provided the response of glycerol uptake to the total-flux sensor is sensitive enough and has its response threshold j_{th} tuned slightly above the uptake flux on glycerol alone, $j_{G,0}$. In the actual system, cAMP–Crp could implement the total-flux feedback strategy. The required sensitive response of glycerol uptake to cAMP–Crp can be achieved by differential regulation of *glpK* and *glpD* by GlpR (see Supplementary Discussion D).

Distinguishing glycolytic and gluconeogenic carbon fluxes—While the total-flux feedback strategy alone can produce the hierarchical and supplementation regimes, it cannot explain the observed simultaneous utilization of gluconeogenic substrates with other substrates[14] because a total-flux sensor does not distinguish glycolytic and gluconeogenic substrates. Specifically, cAMP–Crp signaling is known to respond equally to glycolytic and gluconeogenic substrates (Supplementary Figure 5e)[14].

The situation changes, however, if FBP is added to the scheme. During growth on gluconeogenic substrates the FBP pool is much lower than during growth on glycolytic substrates[24]. Glycolytic and gluconeogenic substrates could therefore be distinguished if the inhibitory effect of FBP on GlpK activity is necessary for the inhibition of glycerol uptake (on top of cAMP–Crp signaling). Consistent with this, a strain carrying the $glpK^{G184T}$ mutation (NQ959), which renders GlpK insensitive to inhibition by FBP[25], lost the hierarchical utilization of glycerol with lactose, instead showing a strikingly linear flux relation (Fig. 5a). We note that the *glpK22* mutation, which renders GlpK insensitive to inhibition by both $EIIA^{Glc}$ and FBP[23], resulted in a similar linear flux relation (Fig. 5a), confirming that $EIIA^{Glc}$ plays a minor role.

Quantitative molecular model of the regulation of glycerol consumption—To verify that specific repression by GlpR, allosteric inhibition of GlpK by upper-glycolytic flux sensor FBP, and total-flux feedback through differential regulation by cAMP–Crp can together account for all experimental observations in Fig. 1 to 4, we constructed a mathematical model; see Supplementary Discussion. For a single set of physiologically reasonable parameters (Supplementary Table 3; see Supplementary Figure 6 for a parameter sensitivity analysis), the model reproduces the threshold-linear flux relation of Fig. 2e, as well as the flux relations of the *ΔglpR*, *glpK22*, and *ΔglpR glpK22* strains (see Fig. 5b).

Moreover, the model predicts the flux relation of the *ΔglpR glpK22* strain to be linear (see Supplementary Discussion B), as observed for the titratable LacY strain in Fig. 5a and the titratable PtsG strain in Extended Data 6a. With the same parameters, the model also reproduces (Extended Data 6) the salient features of the growth-rate crossover seen in Fig. 2a,b, the G3P pool as a function of the growth rate presented in Fig. 3e and 4d, and the response of the *glpK* and *glpD* expression levels as a function of the growth rate shown in Fig. 3b,c.

Simultaneous utilization of glycolytic and gluconeogenic substrates—The model can also predict the growth rate on glycerol + a second substrate (See Supplementary Discussion F, and Extended Data 7a). If the second substrate is glycolytic, the utilization is dictated by the threshold-linear flux relation (Fig. 2e,f), which implies two regimes: (i) If the second substrate provides an uptake flux (and hence growth rate) *larger* than that on glycerol alone, glycerol consumption is fully inhibited, so that the predicted growth rate is simply the growth rate on the second substrate alone. (ii) If the substrate provides an uptake flux (and hence growth rate) *below* that on glycerol alone, glycerol consumption is supplemented such that the growth rate is approximately as obtained on glycerol alone. In contrast, if the second substrate is gluconeogenic, allosteric inhibition of GlpK by FBP is minimal, the substrates are co-utilized, and the resulting growth rate should be *higher* than on each of the individual substrates alone. Note that these predictions do not rely on any details of the model and are completely immune to uncertainty in the model parameters.

To test this, we grew wild-type cells on glycerol plus one of a variety of other substrates. Fig. 5c plots the measured growth rate on two substrates against that on the second substrate alone (colored circles). For second substrates that are processed (at least partly) by the upper-glycolytic pathway (blue circles) the results are consistent with the model prediction (gray band). In contrast, adding a gluconeogenic substrate (orange circles) consistently yields a higher growth than on either substrate alone. We conclude that the joint regulation by FBP and cAMP–Crp limits hierarchical utilization of glycerol to combinations of upper-glycolytic carbon substrates.

Remarkably, a very similar utilization pattern was observed for cells grown on xylose or fucose plus a variety of second substrates (Extended Data 7b,c), suggesting that the regulation strategy of glycerol uptake is not an exception (see Discussion).

DISCUSSION

Flux-based regulation underlies transitions between hierarchical and simultaneous utilization of glycolytic substrates

In this study, we investigated the regulatory strategies underlying the utilization of multiple carbon substrates. Titratable uptake systems allowed us to control the uptake rate of a preferred substrate (lactose or glucose) in the presence of a less preferred one (glycerol) under balanced exponential growth. Glycerol uptake was completely suppressed if the lactose or glucose uptake flux exceeded that on glycerol alone. Otherwise, glycerol uptake was curbed such that the total carbon-uptake flux was maintained near the flux obtained on glycerol alone (Fig. 2c,d). This pattern is reflected by the threshold-linear shape of the flux

relation (Fig. 2e,f) and readily accounts for known differences between batch and continuous cultures: Hierarchical utilization dominates in batch cultures where substrate concentrations and hence uptake rates are high, whereas simultaneous utilization dominates in continuous cultures, where substrate concentrations and hence uptake rates are low.

Flux-based regulation can be efficient because it allows many carbon substrates (glucose, lactose, …) to inhibit the uptake of another substrate (glycerol) through a single regulatory system. As such, it could be used to efficiently establish a hierarchy among a *collection* of substrates (see Supplementary Figure 7). We saw that many pairs of carbon substrates showed a growth-rate crossover similar to those involving glycerol (Extended Data 2), and that the growth rates on xylose or fucose plus a second substrate exhibit the same pattern as observed for glycerol (Extended Data 7b,c). This suggests that a fluxbased mechanism may be employed in the uptake of substrates other than glycerol, although it is unknown whether FBP or another upper-glycolytic flux sensor (*e.g.*, $EIIA^{Glc}$)[26] is involved in those cases. It also justifies the ad hoc rule used in the previous work[27] modeling the kinetics of growth transitions, where a threshold in the total carbon uptake was assumed to control the uptake of less preferred carbon source.

We previously published a very simple model that predicts the growth rate of *E. coli* grown on one glycolytic and one gluconeogenic substrate[14]. Supplementary Figure 8 illustrates the relationship between that model and the one presented here. The mechanistic models developed here are based on knowledge of biological processes. As such, in addition to successfully reproducing complex biological phenomena, they also shed light on the mechanistic origins of these responses.

Total-flux feedback is enabled by differential regulation of two operons

We established that cAMP–Crp causes sharp changes in the pool of inducer G3P (Fig. 4d) through differential regulation of *glpK* and *glpD*. This differential regulation is easily implemented because these enzymes are encoded on different operons. Strikingly, the uptake systems of many other carbon substrates show the same operon organization: separate operons for the enzymes upstream and downstream of the specific inducer, each regulated by cAMP–Crp and a specific repressor. Supplementary Figure 9 illustrates several examples. It is thus possible that the strategy of total-flux feedback through differential regulation is also implemented in these uptake systems.

Also, if the placement of *glpK* and *glpD* in different operons is physiologically important, one would expect this to be preserved in *E. coli*'s pangenome and in related species. An analysis of EcoCyc database (version 23.0) confirmed this[28]. This database returned 300 genomes that contain an ortholog of *glpD* and belong to the order of *Enterobacteriales*. (Of these, 228 are strains of *E. coli*, 38 are other *Enterobacteriacea*, and 34 are *Enterobacteriales* outside of the *Enterobacteriacea*.) In none of these, *glpK* is in the same operon as *glpD*. A similar analysis for the xylose and fucose uptake systems (Extended Data 7b,c) again yielded no exceptions within the *Enteriobacteriales*: the enzymes *xylA* and *xylB* (downstream of inducer D-xylose) are never combined with *xylE*, *xylF*, *xylG* or *xylH* (upstream), and *fucA* (downstream of inducer L-fucose-1-phosphate) is never combined with *fucP, fucI, fucK* or *fucU* (upstream).

In contrast, the famous *lac* system is encoded on a single operon. It is noteworthy, however, that the *lac* system has several exceptional features. First, both our strain (NCM3722) and the strain originally studied by Monod (ML308) grow faster on lactose than on glucose[16,29], but glucose is nevertheless preferred. Thus, cells growing on lactose and glucose cannot possibly follow the growth-rate crossover shown in Fig. 2a,b. Second, the inducer of the *lac* system, allolactose, is synthesized and degraded by one and the same enzyme LacZ, which rules out differential regulation. These features suggest that the *lac* system is an exception to the rule described here.

Physiological rationalization of hierarchical and simultaneous utilization

Recent studies suggest that simultaneous utilization of glycolytic and gluconeogenic substrates is advantageous, allowing cells to save resources that would otherwise be used to express enzymes necessary to connect the upper and the lower parts of carbon catabolism[30–32]. Our study shows that *E. coli* uses the upper-glycolytic sensor FBP as a cue to discriminate glycolytic or gluconeogenic substrates and to choose hierarchical or simultaneous utilization accordingly.

Future experiments of the type presented here for these and other substrates will tell how widely the strategy employing flux sensors is used. Characterization of such strategies for different microbes in a community will reveal a detailed map of who consumes what in which order. It may also open up rational, synthetic biology approaches to manipulating the order of substrate hierarchy, *e.g.*, the efficient breakdown of cellulose for biofuel production[33–35].

METHODS

Reagents and *E. coli* strains

Isopropyl-β-D-1-thiogalactopyranoside (IPTG) was purchased from Bio Basic Inc. (Ontario, Canada). Tetrabuthylammoniumhydrogensulfate (TBAS) was purchased from Waters Corp (Milford, MA). Adenosyne 5'-triphosphate, *o*-nitrophenyl-β-galactoside, 4-amino-antipyrine, N-ethyl-N-(3-sulfopropyl) m-anisidine, chloroacetaldehyde, glycerol 3-phosphate oxidase from *Aerococcus viridans*, horseradish peroxidase, glycerol kinase from *Cellulomonas sp.*, and β-galactosidase from *E. coli* were purchased from Sigma-Aldrich (St Louis, MO). Restriction enzymes were purchased from New England Biolabs (Ipswich, MA).

All *E. coli* strains and oligonucleotides are described in Supplementary Tables 1 and 2, respectively. Unless stated otherwise, all strains were derived from the prototrophic *E. coli* K-12 strain NCM3722[36]. For details on reagents and strain construction, see "Strain construction" below.

Growth conditions

Unless stated otherwise, the nitrogen- and carbon-free minimal-medium base was $N^{-}C^{-}$ as described in Ref. [37]. As nitrogen source, 20 mM of ammonium chloride was used. All growth experiments were conducted at 37°C under vigorous shaking at 250 rpm in a water

bath shaker. In growth-rate measurements and diauxie measurements, each carbon substrate was supplied at the carbon-atom concentration of 120 mM, unless stated otherwise. For measurements of uptake fluxes, the concentrations of carbon substrates were adjusted at each 3MBA concentration such that they were high enough to achieve balanced exponential growth, but low enough to obtain sufficient resolution for uptake measurements (see Source Data). OD_{600} was measured with a spectrophotometer Genesys 20 (Thermoscientific). With this spectrophotometer, one OD_{600} × ml is equivalent to 0.44 mg dry weight[38].

Strain construction

Transfer of *glpK* mutations to NCM3722 background—The *glpK* point mutations *glpK22* and $glpK^{G184T}$ were moved from one strain to another as follows. A kanamycin-sensitive parental strain was first transduced with P1*vir* phage prepared from JW3887–1 (Δ*pfkA775*::*kan*). The kanamycin-resistant *pfkA* transductant cannot grow on minimal agar plates supplemented with 20 mM mannitol as the sole carbon substrate [39]. The *pfkA* transductant was further transduced with P1*vir* phage prepared from the *glpK* mutant strain and selected on the minimal agar plate supplemented with 20 mM mannitol as the sole carbon substrate. Since *pfkA* and *glpK* are genetically linked, the *glpK* mutant frequently replaces the wild-type *glpK* in Mtl^+ ($pfkA^+$) transductants. The Mtl^+ Kan^S transductant carrying the *glpK* allele of interest was selected by DNA sequencing of the region surrounding the mutation.

$P_{LtetO-1}$-*xylR*—The $P_{LtetO-1}$-*xylR* allele was made as follows. The *xylR* gene [40] was cloned as a *KpnI-BamHI* fragment on pKD13-*rrnBt*:$P_{Ltet-O1}$ [41]. The resulting plasmid was used as a template to insert a tandem array of the *kan* gene, the *rrnB* terminator, and $P_{LtetO-1}$:*xylR* between *ycaC* and *ycaD* (*zca* locus) and between *intS* and *yfdG* (*zfd* locus) by primer sets ycaD-P1-S1 & ycaD-P4-A1 and intC-P1-S1 & intC-P4-A1, respectively. P1*vir* phages were prepared from these strains and used to transduce NCM3722. Using these phages, NQ914 and NQ915 were created by respectively one and two cycles of transduction and the flip-out of the *kan* gene.

P*u*-*ptsG*—The Δ*ptsG468*::Φ(*kan*:P*u*) allele in which the *ptsG* promoter is replaced by the P*u* promoter was made as follows. The region containing the *kan* gene and P*u* promoter was PCR amplified by primers SDY158 and SDY159 from NQ381[16] and integrated at the *ptsG* locus, resulting in the replacement of 342 base before the open reading frame with a tandem array of *kan* gene and P*u* promoter (*zah* locus) by using the λ Red system [42], which results in the replacement of *ptsG* promoter with P*u* promoter.

glpFp-gfp—NQ1344 was made as follows. The plasmid pKD13-*rrnBt*:$P_{Ltet-O1}$:*gfp* was made by inserting the *gfpmut3b* structural gene immediately downstream of the $P_{LtetO-1}$ promoter in pKD13-*rrnBt*:$P_{Ltet-O1}$ [41]. The $P_{LtetO-1}$ in the plasmid pKD13-*rrnBt*:$P_{Ltet-O1}$:*gfp* was replaced by an *XhoI-KpnI* fragment containing the *glpF* promoter that was amplified from NCM3722 by primers PglpF-XhoI-S2 and PglpF-KpnI-A4. The resulting plasmid pKD13-*rrnBt*:*glpFp*:*gfp* was used to produce a donor DNA fragment. The host strain was made by flipping out the *kan* gene from the strain carrying a tandem array of *kan* gene, *rrnB* terminator, *glnK* promoter, the 5' untranslated region (5' UTR) from the $P_{LtetO-1}$ promoter

and the structural gene of *gfpmut3b* between *intS* and *yfdG* (*zfd* locus) [43] and transforming the flipped-out strain with pKD46 for λ Red recombination [43]. This strain was transformed with the donor DNA fragment that was amplified by primers intC-P1-S1 and gfp-Ptet-PglpF-A1 using pKD13-*rrnBt*:*glpFp*:*gfp* as a template. The resulting strain carries a tandem array between *intS* and *yfdG* consisting of the *kan* gene, the *rrnB* terminator, the *glpF* promoter spanning −246 to −1, the 5' UTR from $P_{LtetO-1}$ promoter, and the structural gene of *gfpmut3b*. P1*vir* phage was prepared from this strain and used to transduce the strain with the *kan* gene flipped out from NQ916.

***glpFp-lacZ* and *glpDp-lacZ*—**The *glpFp-lacZ* reporter strain HE305 was made by transducing NQ1332, a strain made by flipping out of *kan* gene from NQ1243, with P1*vir* phage containing a tandem array of the *kan* gene, the *rrnB* terminator, and the *glpF* promoter spanning −273 to −1 bp relative to *glpF* translational start site[16].

The *glpDp-lacZ* reporter strain HE397 was made as follows. The $P_{LtetO-1}$ in the plasmid pKD13-*rrnBt*:$P_{Ltet-O1}$ was replaced with an *XhoI-KpnI* fragment containing the *glpD* promoter that was amplified from NCM3722 by primers PH008 and PH009. The resulting plasmid pKD13-*rrnBt*:*glpDp* was used to produce a DNA as follows. First, a DNA fragment was amplified by PH019 and PH020 using pKD13-*rrnBt*:*glpDp* as a template. This fragment was further amplified by primers PH025 and PH026 to produce the DNA donor. The host strain NQ309 was transformed with the donor DNA fragment to replace a part of *lacI* gene and the entire *lac* promoter (from +134 bp after *lacI* translational start codon to *lacZ* translational start codon) with a tandem array of the *kan* gene, the *rrnB* terminator, and the *glpD* promoter spanning −292 to −1 bp relative to *glpD* translational start site. P1*vir* phage was prepared from this strain and used to transduce NQ1332 to obtain HE397.

Measurements of glucose, lactose, and glycerol uptake

A fraction of an exponentially growing culture was collected and kept on ice for < 0.5 h. The incubation on ice caused a decrease in the concentration of each carbon substrate by only 2–3%. After the sample was centrifuged at 16,110 × g for 1 min, the supernatant was taken, frozen on dry ice and kept at −80°C. Typically, four samples were taken at OD_{600} between 0.15 and 0.60.

Glucose was assayed enzymatically using a commercially available kit (Glucose Assay Kit, GAHK20; Sigma-Aldrich). For the lactose assay, samples were first digested by β-galactosidase in Z-buffer at 37°C for 20 min and the released glucose was measured using the glucose assay described above. As a control, the sample was treated in the same way without β-galactosidase. Little glucose was detected in the control. Glycerol was measured essentially as described in Ref. [44]. The assay was performed by adding 7.5 μl sample to 225 μl reaction mixture containing 50 mM MOPS [pH7.0], 0.75 mM ATP, 3.75 mM $MgSO_4$, 0.188 mM 4-aminoantipyrine, 2.11 mM N-ethyl-N-(3-sulfopropyl) m-anisidine, sodium salt, 2.5 U/ml glycerol phosphate oxidase, and 2.5 U/ml peroxidase with or without 1.25 U/ml glycerol kinase. After incubation at room temperature for 30–60 min, A_{540} was measured and converted to the glycerol concentration based on standards.

The carbon-uptake rate was calculated as the slope of carbon concentration versus OD_{600}, multiplied by the specific growth rate.

G3P pool measurements by enzymatic assay

G3P pools reported in Fig. 4d were measured as follows. The culture of NQ1187 was grown to OD_{600} = 0.5, and the cells were harvested by filtration of 2.5 ml culture through the membrane filter (25 mm-disc with 0.45 μm pore size, HAWP02500; Millipore) pre-wetted with warmed culture medium, and washed by 2.5 ml warmed culture medium. The filter was quickly immersed in 4 ml of extraction solution (40% (v/v) methanol, 40% (v/v) acetonitrile, and 20% (v/v) water) precooled at −20°C, and incubated at −20°C for 2 h. The extract was dried in a vacuum concentrator and stored at −80 °C. Immediately prior to the assay, the samples were dissolved in 170 μl phosphate-buffered saline (D1408; Sigma-Aldrich). G3P was assayed enzymatically using a commercially available kit (Amplite Fluorimetric Glycerol 3-Phosphate Assay Kit, 13827; AAT Bioquest).

Measurements of intracellular metabolites by mass spectrometry

G3P and FBP pools reported in Fig. 3e and Fig. 4a,b were measured as follows. Cultivations were performed in M9 minimal media in 96-deep-well plates as described in[24]. During mid-exponential phase (OD_{600} = 0.5), cells were harvested by fast filtration using 1 mL culture as described previously[24], and the filter was quickly immersed in 4 ml of extraction solution (40% (v/v) methanol, 40% (v/v) acetonitrile, and 20% (v/v) water) precooled to −20°C and incubated at −20°C for 2 h. Samples were dried completely at 120 lbar (Christ RVC 2–33 CD centrifuge and Christ Alpha 2–4 CD freeze dryer), and stored at −80°C until measurements. Before measurements, samples were resuspended in 100 μL water, centrifuged for 5 min (5,000 × g, 4°C) to remove residual particles, diluted 1:10 in water, and transferred to V-bottomed 96 well sample plates (Thermo Fisher Scientific). Samples were measured by flow-injection time-of-flight mass spectrometry with an Agilent 6550 QToF instrument operated in negative ionization mode at 4 GHz high-resolution in a range of 50–1,000 m/z as described before[45]. Sample processing and ion annotation was performed based on accurate mass within 0.001 Da using the KEGG eco database[46] as reference and accounting for single deprotonated forms of the respective metabolite (M-H+) as described before[46].

Total and lactose uptake rates used to plot (in Fig. 4a, b) against FBP pools were estimated from the relation between uptake rates [ℂ] and 3MBA concentrations [μM] in Fig. 2c. Lactose uptake rates above 12.5 μM 3MBA on lactose + glycerol and lactose alone were estimated as $-0.495 \times \ln([3MBA])^3 + 6.326 \times \ln([3MBA])^2 - 18.745 \times \ln([3MBA]) + 23.499$ and $0.252 \times \ln([3MBA])^3 - 3.446 \times \ln([3MBA])^2 + 18.452 \times \ln([3MBA]) - 9.881$, respectively. Glycerol uptake rates on lactose + glycerol below and above 100 μM 3MBA were estimated as $34.091 - 6.679 \times \ln([3MBA])$ and 0, respectively. When estimating uptake rates at 0 μM 3MBA, we used 10 μM (instead of 0 μM) in the natural logarithm.

Single-cell analysis of GFP expression from the *glpF* promoter

Cultures of strain NQ1344, carrying a chromosomal *glpFp-gfp* reporter gene together with the titratable LacY system, were grown on N^-C^- medium supplemented with 20 mM

NH_4Cl, 3 mM lactose (Supplementary Figure 2a, c–l) or 10 mM lactose (Supplementary Figure 2b,n), and 4 mM glycerol (Supplementary Figure 2c–e) or 8 mM glycerol (Supplementary Figure 2f–k, n). At OD_{600} = 0.5, a fraction of the culture was taken and kept on ice until images were taken. GFP fluorescence and phase contrast (PC) images were acquired by a Clara charge-coupled device camera (Andor, Belfast, UK) for Supplementary Figure 2c–l or QImaging Retiga 2000R MONO (Teledyne Qimaging, Surrey, Canada) for Supplementary Figure 2n connected to an Eclipse Ti inverted microscopic system (Nikon Inc., Melville, NY) under the control of NIS Elements software (Nikon Inc., Melville, NY).

Images were analyzed using the open-source platform software Fiji[47] as follows. Individual cells were identified as region of interest (ROI) on a PC image with an appropriate threshold set. To minimize the number of misidentified cells, the gate for the cell size was set with the ratio of maximal to minimal cell size set to 4, and remaining misidentified cells were manually removed. The ROIs thus obtained on a PC image were overlaid to the corresponding GFP fluorescence image and mean intensity in each ROI was measured. For series A (see Supplementary Figure 2) background fluorescence was subtracted from the signal and used to normalize the intensities. For series B, no background was subtracted; instead, the fluorescence level of cells grown on lactose only with 500 μM of 3MBA was measured to determine the fluorescence level of cells with minimal *glpFp* expression.

Glycerol kinase assay

Cell extracts were prepared essentially as described before [17]. A 25 mL culture was grown exponentially until OD_{600} = 0.5. Twenty mL of the culture was transferred to a tube precooled on ice water and chloramphenicol was added to give a final concentration of 40 μg/mL. The cells were harvested by centrifugation at 0°C, washed with 40 mL of 1% NaCl, resuspended in 200 μL extraction buffer containing 0.1 M MOPS-NaCl at pH7.0, 1 mM 2-mercaptoethanol, 1 mM ethylenediaminetetraacetic acid, and 2 mM glycerol, and stored at −80°C.

Before the assay, the cell suspension was thawed, disrupted by sonication on ice water for 4 times 5 s at the amplitude of 4 at low mode in a MSE sonicator, centrifuged at 13,600 × g for 30 min at 4°C, and the supernatant was frozen at −80°C. The GlpK activity was stable for one day at −80°C.

The cell extract was thawed immediately before the assay and diluted in the extraction buffer. The reaction was started by adding 40 μL of cell extract to 200 μL of assay buffer, both of which were preincubated at 37°C for 5 min, to give final concentrations of 0.1 M MOPS-NaCl at pH7.0, 0.167 mM 2-mercaptoethanol, 0.167 mM ethylenediaminetetraacetic acid, 2 mM glycerol, 2.5 mM ATP, 13.5 mM $MgSO_4$, 0.188 mM 4-aminoantipyrine, 2.11 mM N-ethyl-N-(3-sulfopropyl) m-anisidine, 5 U/mL glycerol phosphate oxidase, and 5 U/mL peroxidase. A_{540} was recorded every 6 s. To confirm that the activities were proportional to the concentrations of the cell extracts added to the reaction mixture, the assays were repeated with four different dilutions of the cell extract for each. The GlpK activity was reported as A_{540} per min per mg of total protein. Total amounts of protein in a cell extract were determined by Biuret method [48].

cAMP assay

The cAMP concentrations in media were assayed as described before [16].

A fraction of an exponentially growing culture was collected and filtered through a 0.22-μm-pore-size nylon membrane filter, and the filtrate was frozen on dry ice and kept at −80°C. Four samples were taken at OD_{600} between 0.15 and 0.60.

cAMP in the filtrate was ethenylated by incubation of 80 μL filtrate for 30 min at 70°C in the presence of 1.2 M chloroacetaldehyde, 25 mM Na_2HPO_4 [pH 4.0], and 5 mM EDTA in a final volume of 200 μL. The reaction mixture was transferred to ice, neutralized by adding one-third volume of 0.5 M NH_4HCO_3, filtered through a 0.22-μm-pore-size nylon membrane filter, and analyzed by high performance liquid chromatography (HPLC). The HPLC system used was Shimadzu Prominence HPLC system composed of LC-20AB binary pump, SIL-10AF autosampler, and RF-10AxL fluorescence detector as main modules. Eluent flow rate was 1.5 mL/min. The eluent used was a TBAS buffer (5.7 mM TBAS, 30.5 mM KH_2PO_4 adjusted to pH 5.8 with phosphoric acid) and an acetonitrile buffer (acetonitrile:TBAS buffer, 2:1). Seventy μL sample aliquot was injected on XTerra MS C18 column (3.0 × 50 mM, I.D. 3 mM, 5 μm particle size; Waters Corp.) equipped with its guard column and maintained at 40°C during separation. The elution was isocratic with 90% TBAS buffer (10% acetonitrile buffer) for 3 min after injection, decreased to 50% TBAS buffer in 3 sec, remaining isocratic for 1.9 min, and re-equilibrated with 90% TBAS buffer for 2 min. The fluorescence signal was monitored at an excitation wavelength of 280 nm and an emission wavelength of 410 nm. Ethenylated cAMP typically eluted between 1.5 and 1.6 min.

The cAMP excretion rate was calculated as the slope of the plot of cAMP concentration in a filtrate versus OD_{600}, multiplied by the specific growth rate.

Statistics and Reproducibility

Fig. 1: The data shown in Panel a and b are from a single series of experiments.

Fig. 2: In all panels, each datapoint derives from a single experiment. In Panels a and b, a complete data series (composed of 18 datapoints in total: the growth rates on lactose/glucose, glycerol, and both, each at six 3MBA concentrations) was typically obtained through two independent batches of experiments. In Panel a, this two-batch series was repeated and hence two data series are shown for each carbon substrate. The full dataset in Panels c and e was obtained through ten independent batches of growth-rate measurement and sampling which include replicates of the same or similar culture conditions, seven independent batches of the lactose uptake measurements, and seven independent batches of the glycerol uptake measurements. The full dataset in Panels d and f was obtained through four independent batches of growth-rate measurement and sampling which include replicates of the same or similar culture conditions, five independent batches of lactose uptake measurements, and four independent batches of glycerol uptake measurements. See Source Data for details.

Fig. 3: In all panels, each datapoint derives from a single experiment. The full dataset in Panel b was obtained through six independent batches of growth-rate measurements and sampling, and six independent batches of LacZ assays. The full dataset in Panel c was obtained through four independent batches of growth-rate measurements and sampling, and four independent batches of LacZ assays. The full dataset in Panel d was obtained through eight independent batches of growth-rate measurement and sampling which include replicates of the same or similar culture conditions, seven independent batches of lactose uptake measurements, and seven independent batches of glycerol uptake measurements. The full dataset in Panel e was obtained through three independent series of growth-rate measurement and sampling which include replicates of the same culture conditions and two independent sets of mass spectrometry experiments. See Source Data for detail.

Fig. 4: In all panels, each datapoint represents a single experiment. The full dataset in Panel a and b was obtained through three independent batches of growth-rate measurements and sampling which include replicates of the same culture conditions and two independent sets of mass spectrometry experiments. In Panel c and d, the full datasets were obtained through two independent batches of sampling and a single batch of measurement. See Source Data for detail.

Fig. 5: In Panel a, each datapoint represents a single experiment and the full datasets for *glpK*^{G184T}, *glpK22*, and *ΔglpR glpK22* were obtained through six, six, and three independent batches of growth-rate measurement and sampling, respectively, which include replicates of the same or similar culture conditions, five, four, and one independent batches of lactose uptake measurements, respectively, and five, five, and one independent batches of glycerol uptake measurements, respectively. In Panel c, the *x*- and *y*-values of each datapoint represents the average of the growth rates obtained from at least two independent experiments. See Source Data for details.

Extended Data 1: In Panels a and d, the growth experiments were repeated twice and similar growth curves were obtained as shown in Source Data. In the other panels, each data set shown derives from a single experiment.

Extended Data 2: In all panels, each datapoint derives from a single experiment. A full data series, composed of the growth rates on three carbon-substrate conditions (1st substrate, 2nd second substrate, and both) at six (Panel a-e) or seven (Panel i) 3MBA concentrations (18 or 21 datapoints in total) was typically obtained through two independent batches of experiments. In Panel a, this two-batch series was repeated and hence the two datasets are shown for each carbon substrate.

Extended Data 3: Each growth curve derives from a single experiment.

Extended Data 6: In Panel a, each datapoint derives from a single experiment and the full dataset was obtained through four independent batches of growth-rate measurements and sampling which include replicates of the same or similar culture conditions, four independent batches of the lactose uptake measurements, and four independent batches of the glycerol uptake measurements. See Source Data for details.

Extended Data 7: In Panel b and c, the *x*- and *y*-values of each datapoint represents the average of the growth rates obtained from two independent experiments. See Source Data for details.

Reporting Summary

Further information on research design is available in the Nature Research Reporting Summary linked to this article.

DATA AVAILABILITY

The datasets corresponding to all figures (including Extended Data Figures and Supplementary Figures) are available online as Source Data.

CODE AVAILABILITY

Numerical analyses of the mathematical model were carried out using Wolfram Mathematica 11.3, gnuplot, and R (version 3.5.1). A Mathematica notebook that reproduces the central modeling results is shared at: https://doi.org/10.5281/zenodo.3462129. Other code will be shared upon reasonable request.

Extended Data

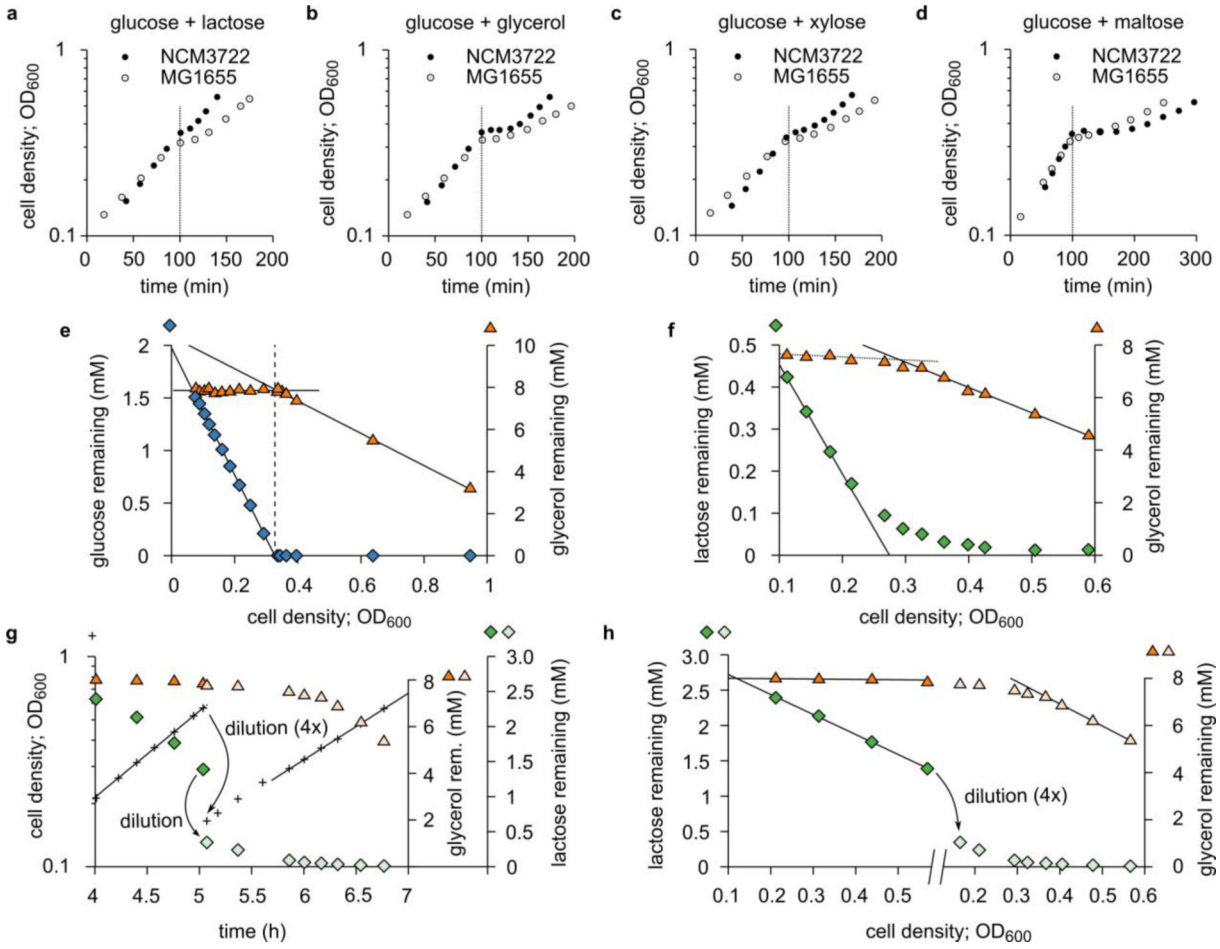

Extended Data Figure 1. Examples of diauxic ("double growth") curves.

a—d. Diauxic growth curves[1] on glucose and one additional carbon substrate, for *E. coli* strains NCM3722 (closed circles) and MG1655 (open circles). A diauxic curve consists of two exponential growth phases separated by a lag phase during which the culture hardly grows. (For comparison, all data series are shifted horizontally such that the lag begins at ~100 min.)

The duration of the lag phase varies between strains and substrate pairs, from a few minutes (NCM3722 in Panel a) to over an hour (NCM3722 in Panel d).

e. Hierarchical growth on glucose plus glycerol. The same data as Fig. 1a are now plotted against OD_{600}. The glucose concentration (blue diamonds) initially decreases *linearly* (black solid lines are linear fits): during balanced exponential growth, producing a unit of cell mass consumes a fixed amount of substrate. After glucose runs out, glycerol (orange triangles) is consumed, again linearly.

f. Similar to Panel e, but with lactose (green diamonds) instead of glucose, using the same data as Fig. 1b. Here, the transition to glycerol utilization is more gradual than Panel e. Lactose uptake slows down before lactose is used up, likely due to the large Michaelis constant of the lactose permease[50]: K_M = 0.1 to 1 mM. The reduction in lactose uptake relieves the inhibition of glycerol uptake before lactose is fully depleted, resulting in a smooth transition. In contrast, the K_M of the glucose transporter PtsG[51,52] is 3—10 μM;

therefore, cells do not sense that glucose is running out until the glucose concentration is very low (Panel e and Fig. 1a).

g. As Fig. 1b, except the higher initial lactose concentration (3 mM instead of 0.7 mM) to fully inhibit glycerol uptake. To observe the transition to glycerol utilization before the culture reaches high OD_{600}, the culture was diluted, at OD_{600} = 0.5, four-fold in fresh medium containing glycerol (green diamonds before dilution, pale-green diamonds after) but no lactose (orange triangles before dilution, pale-orange triangles after).

h. Same data as Panel g, except that lactose and glycerol concentrations are plotted against OD_{600}, revealing straight lines similar to Panel e and f.

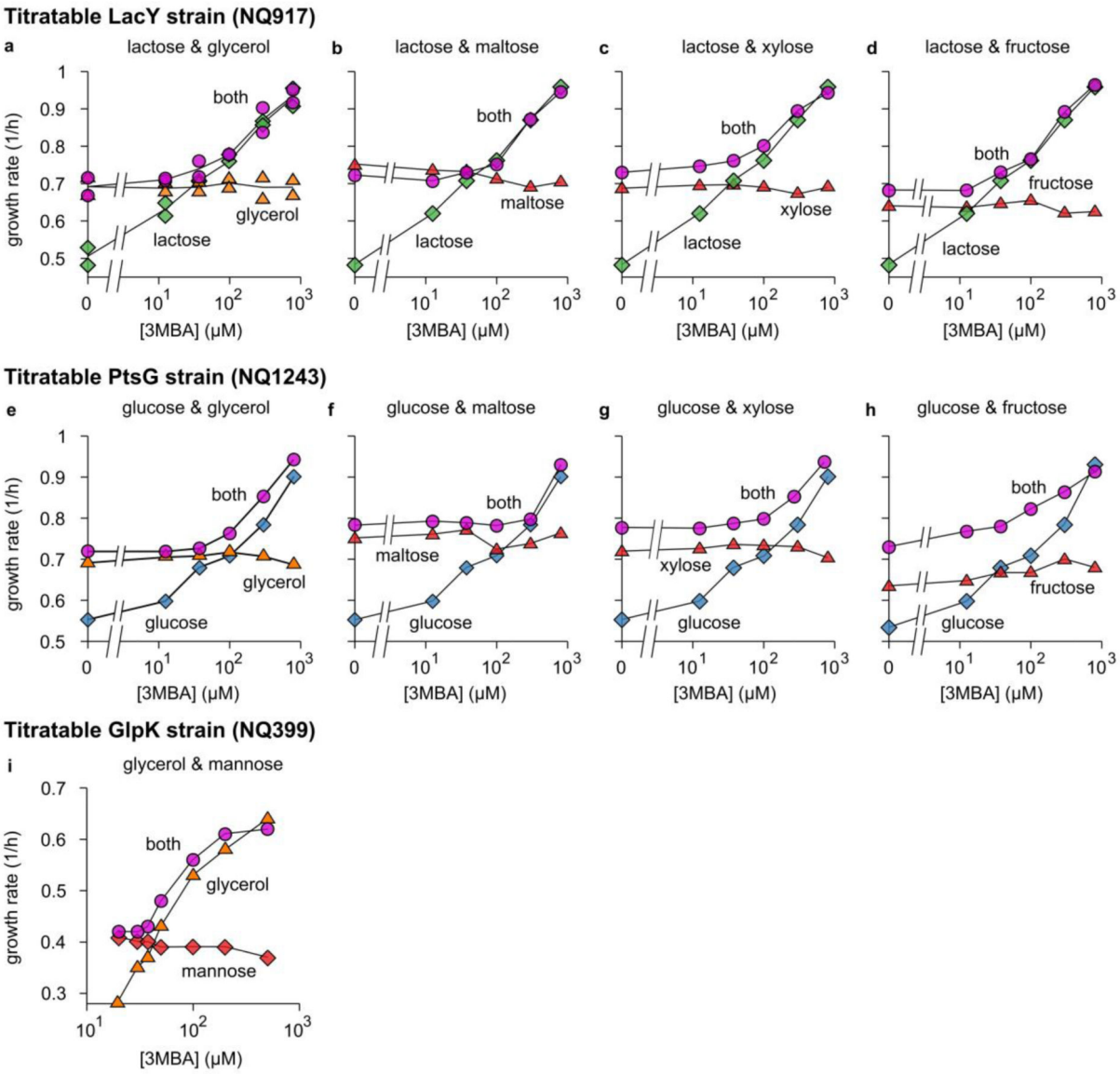

Extendend Data Figure 2. Growth-rate crossover patterns for various combinations of substrates.

a—d. The growth rate of the titratable LacY strain (Supplementary Figure 1a) grown on lactose and a second substrate (glycerol, maltose, xylose or fructose) as a function of 3MBA concentration. Each plot shows the measured growth rate on lactose only (green diamonds), the growth rate on the second substrate only (orange or red triangles), and the growth rate in the presence of both (pink circles).

e—h. As Panels a—d, but for the titratable PtsG strain (Supplementary Figure 1b) and glucose (green diamonds) instead of lactose.

i. Similar results for the titratable GlpK strain (Supplementary Figure 1c) growing on glycerol (orange triangles), mannose (red diamonds), or both (pink circles).

In all cases (Panels a—i), if the 3MBA concentration is reduced sufficiently, the growth rate on the preferred carbon substrate eventually becomes smaller than the growth rate on the non-preferred one. Yet, the growth rate in the presence of both substrates never drops below

the growth rate on the non-preferred one, indicating that the uptake of the non-preferred substrate is induced. In almost all cases, the crossover regime is rather narrow. The glucose-fructose hierarchy is an apparent exception.

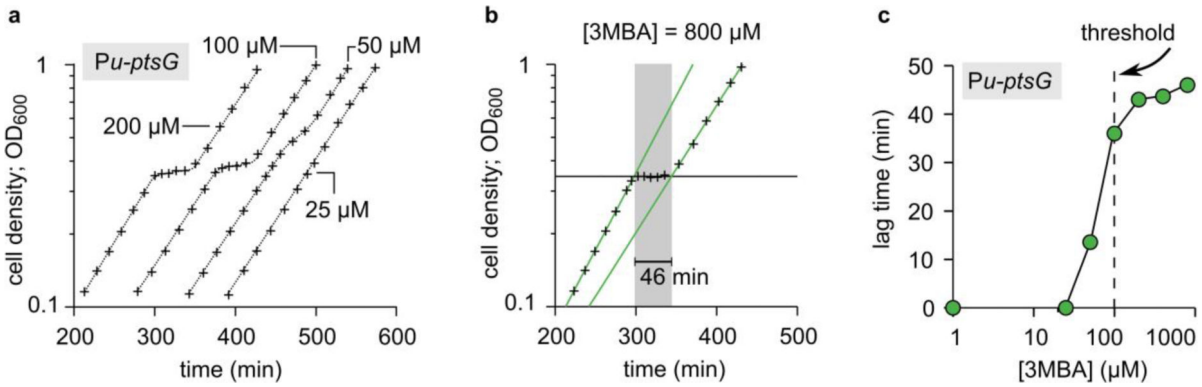

Extended Data Figure 3. The diauxic lag disappears in the supplementation regime.

a. Diauxic growth curves (+) of the titratable PtsG strain (NQ1243) in medium with 1.7 mM glucose and saturating glycerol. Each curve is for a different 3MBA concentration (indicated in the figure) and horizontally shifted for convenience. The data shown is from a single series of experiments.

b. Lag times were determined for each diauxic growth curve; the method is illustrated here using the condition [3MBA] = 800 μM as an example. We fitted exponential curves through the two growth phases (green lines) and a horizontal line through the lag phase (horizontal black line). The lag time (indicated in gray) is heuristically defined as the horizontal distance between the intersections of the green lines with the horizontal one. In this case, a lag time of 46 minutes is found.

c. Lag times of the growth curves versus [3MBA]. The diauxic lag time vanishes precipitously when [3MBA] is tuned below 100 μM, where glycerol and glucose are co-utilized.

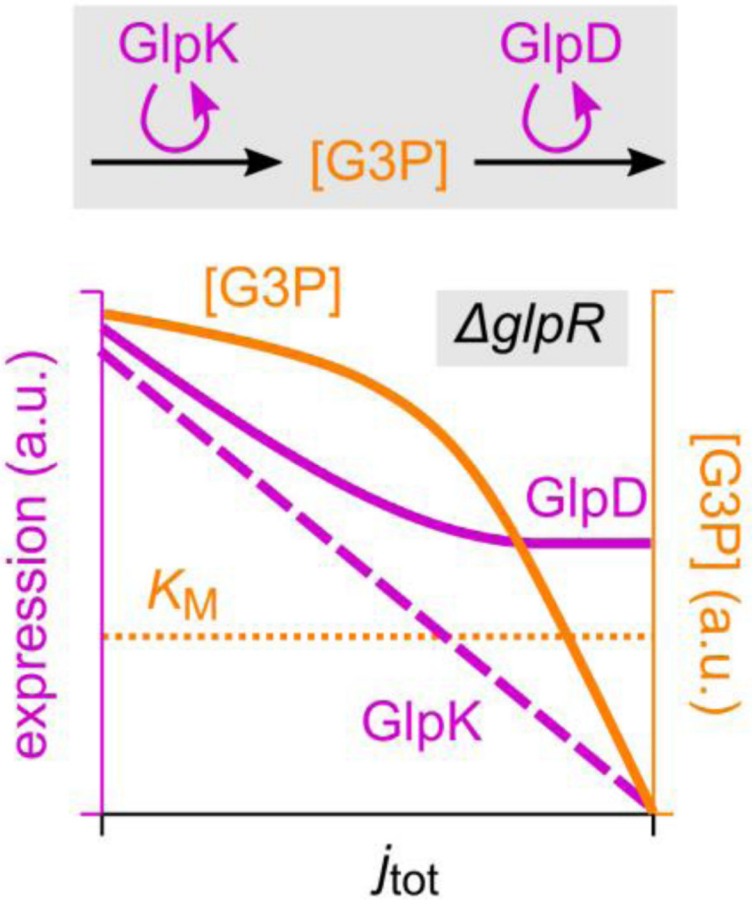

Extended Data Figure 4. How differential regulation by cAMP-Crp can affect G3P concentration.

As demonstrated in Fig. 3b,c using the *ΔglpR* and *ΔglpR glpK22* background, cAMP-Crp signaling affects the expression of the *glpK* and *glpD* genes differently: with increasing growth rate (decreasing cAMP-Crp transcriptional activation), *glpK* expression vanishes whereas *glpD* expression maintains a significant basal level. The figure illustrates how this differential regulation explains the marked growth-rate dependence of the G3P concentration observed in the *ΔglpR glpK22* background (Fig. 4d).

G3P is the product of GlpK and the substrate of GlpD. The synthesis of G3P should therefore be proportional with the abundance of GlpK, while its turnover increases with both GlpD abundance and substrate concentration [G3P]. Flux balance then implies that [G3P] increases with the ratio of GlpK (purple dashed line; sketch based on Fig. 3b) to GlpD abundance (purple solid line; sketch based on Fig. 3c). This ratio reduces with increasing growth rate, so that the G3P concentration (solid orange line; sketch) reduces as well.

In strains without the *ΔglpR* mutation the same mechanism should act, but with an additional layer of amplification: Because both *glpK* and *glpD* expression are repressed by GlpR, an increase in its inducer G3P due to differential regulation has little effect until it is of the order of the Michaelis constant K_M (horizontal dotted line) associated with the induction of GlpR, upon which *glpK* and *glpD* expression are induced and glycerol uptake is turned on.

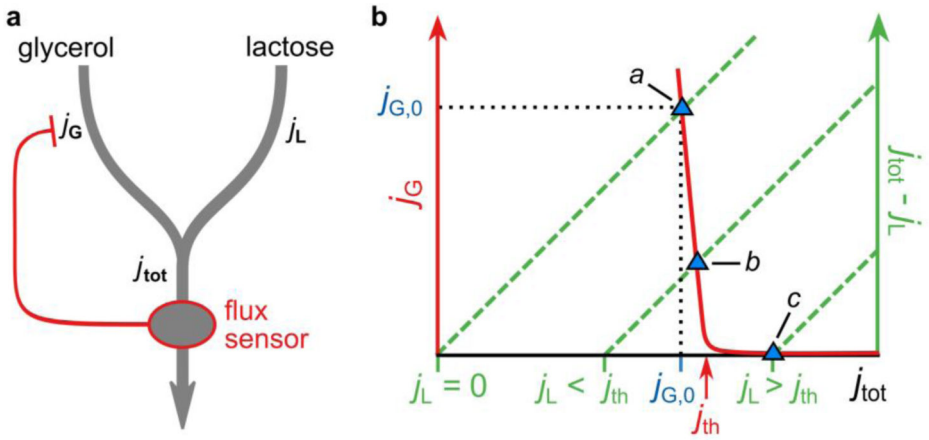

Extended Data Figure 5. The total-flux feedback model.

Several key observations can be explained by a highly simplified regulatory scheme in which glycerol uptake is inhibited by a signal that reflects the total carbon-uptake flux—a *total-flux sensor*. In this scheme (Panel a), glycerol and lactose uptake j_G and j_L both contribute to the total carbon-uptake flux j_{tot}. This total flux is sensed by a total-flux sensor, which represses glycerol uptake, but only if j_{tot} exceeds a threshold that is set to coincide with the carbon flux obtained on glycerol alone. Thus, glycerol uptake is suppressed by any substrate that supplies a larger carbon-uptake flux than glycerol can provide, but not by substrates that produce a smaller flux.

Panel b demonstrates graphically how total-flux feedback determines the uptake of glycerol. Because $j_G = j_{tot} - j_L$, the steady-state value of j_G obtained for a given j_L can be found by plotting both $j_G(j_{tot})$ (red solid curve) and $j_{tot} - j_L$ (green dashed lines, for various values of j_L) as a function of j_{tot} and determining their intersection (blue triangles). We assume that j_G responds sensitively to j_{tot}, with a threshold j_{th} (red arrow) set slightly above the flux on glycerol alone, $j_{G,0}$. Thus, it is seen that glycerol uptake is inhibited if $j_L > j_{th}$ (the hierarchical utilization regime, intersection *c*). Yet, if $j_L < j_{th}$, glycerol uptake is adjusted such that $j_{tot} \approx j_{th} \approx j_{G,0}$ (the supplementation regime; intersection *a* and *b*).

cAMP–Crp signaling can function as a total-flux sensor because transcriptional activation by cAMP–Crp is a decreasing function of j_{tot} (Fig. 4c)[5]. It transmits information on j_{tot} to the glycerol uptake through differential regulation of *glpK* and *glpD* expression (Fig. 3b,c).

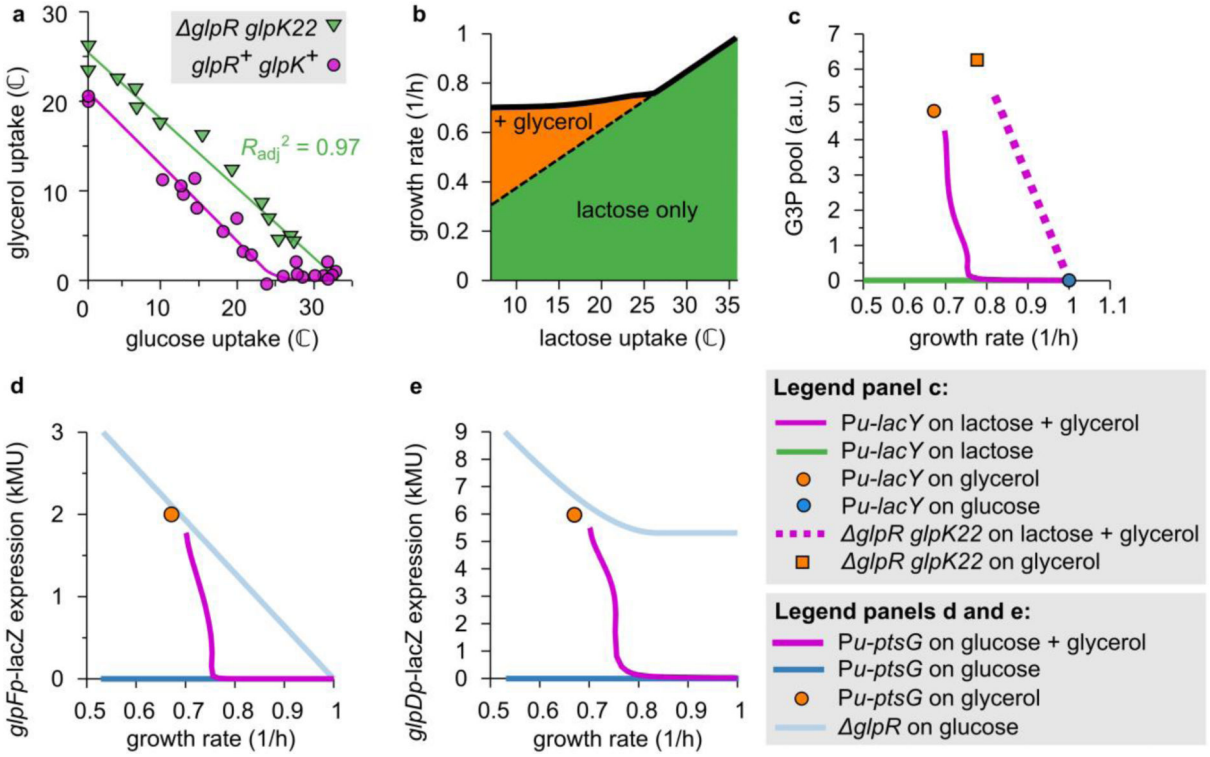

Extended Data Figure 6. Model predictions.

With a single parameter set, our mathematical model reproduces the main features of various measurements in addition to the flux relations of the various mutants (Fig. 5b).

a. The flux relation of the titratable PtsG strain with the *ΔglpR glpK22* mutations (NQ1264) is linear (Pearson correlation:$R^2_{\text{adj}} = 0.97$, $n = 13$ experimental conditions, $t = 21$, df = 11, $p = 3 \times 10^{-10}$), as predicted by the model. The flux relation for the *glpR*$^+$ *glpK*$^+$ strain (NQ1243) is also plotted for comparison.

b. The growth-rate crossover of the titratable LacY strain. The model predicts that, on lactose only, the growth rate decreases linearly (dashed line) on lactose only as lactose uptake (green area) is reduced.. On lactose and glycerol, the growth rate initially follows the same trend (solid line), but below the threshold lactose flux of ≈ 25 ℂ glycerol uptake (orange area) is gradually induced such that the growth rate remains approximately constant. This behavior underlies the observations in Fig. 2a and c. (The model makes identical predictions for the titratable PtsG strain.)

c. The G3P pools. The model predicts that in the titratable LacY strain grown on lactose + glycerol (purple solid line), as the lactose uptake is reduced, the G3P pool remains low until the growth rate approaches that on glycerol only, ≈ 0.7/h; it then sharply increases and converges to the level obtained during growth on glycerol only (orange circle). This closely resembles the measured behavior in Fig.3e (purple and orange circles). The sensitive response is disrupted in the *ΔglpR glpK22* double mutant (purple dotted line and orange square), in agreement with Fig. 4d (purple and orange squares).

d-e. Expression from *glpF* and *glpD* promoters. If the titratable PstG strain is grown on glucose + glycerol and glucose uptake is reduced, expression levels from both *glpF* and *glpD* promoters are negligible until the growth rate approaches the growth rate on glycerol only,

~0.7/h (purple solid lines in both figures). The sudden onset of expression is completely lost in the *ΔglpR* mutation strain (light blue curves in both figures). This agrees with the measured expression levels in Fig. 3b and c.

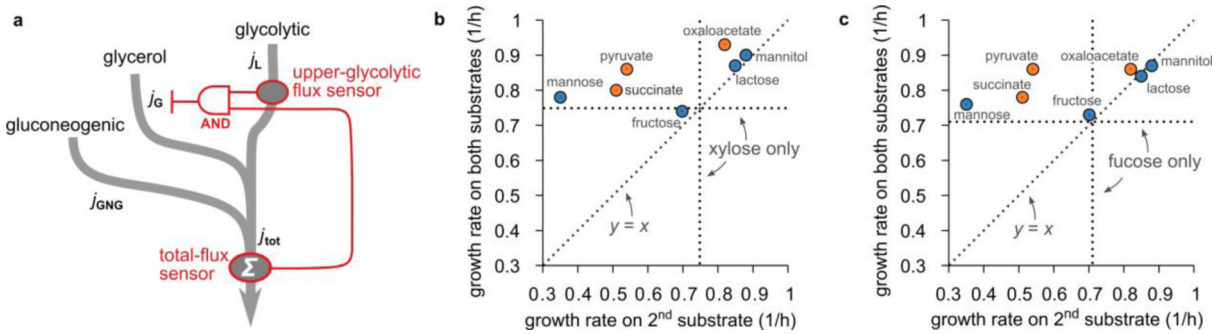

Extended Data Figure 7. Growth on glycerol, xylose or fucose with various second substrates.

a. This diagram illustrates the difference in the effect of glycolytic and gluconeogenic substrates on glycerol uptake. The uptake and catabolism of glycerol, gluconeogenic substrates and glycolytic substrates are drawn as three pathways (gray arrows) that merge at different places. In the regulation (red lines), two flux-sensors are involved: one (FBP) senses the upper-glycolytic flux j_L, the other (cAMP-Crp) the total carbon flux j_{tot}. Crucially, both flux sensors are required to fully suppress glycerol uptake; this is symbolized in the diagram using the symbol of a logical AND gate. Glycolytic substrates contribute both to the upper-glycolytic flux and the total carbon flux. A sufficiently large glycolytic flux therefore activates both the upper-glycolytic flux sensor AND the total-flux sensor, which together suppress glycerol uptake. In contrast, gluconeogenic substrates do not contribute to the upper-glycolytic flux and will not fully inhibit glycerol uptake even if they provide a large carbon flux. (Through the total-flux sensor cAMP-Crp, gluconeogenic substrates will affect glycerol uptake mildly, but both substrates remain co-utilized.) This difference between glycolytic and gluconeogenic substrates underlies the pattern in Fig. 5c.

b. A pattern similar to Fig. 5c is obtained if glycerol is replaced by xylose. Shown here is the growth rate of WT cells (NCM3722) in M9 medium[24] on xylose plus a second substrate plotted against growth rate with the second substrate only, for a variety of “second” substrates. The growth rate on xylose only is indicated by horizontal and vertical dotted lines. The growth rate on both substrates shows a similar dependence on the “second” substrate species as seen in Fig. 5c of the main text: If the second carbon substrate is processed at least partially by upper glycolysis (blue circles) the growth rate is approximately the larger of the two single-substrate growth rates, possibly with an exception for mannose. If on the other hand the second substrate is a gluconeogenic substrate (orange circles) the growth rate on both substrates is usually larger than either of the two single-substrate growth rates.

c. Same as Panel b, but for fucose as the “first” substrate.

Supplementary Material

Refer to Web version on PubMed Central for supplementary material.

ACKNOWLEDGEMENTS

We are grateful to Uwe Sauer for his generous support and encouragement, to Thomas Egli, Luca Gerosa, Joshua Silverman, and members of the Hwa lab for helpful discussions, to Kenyon Applebee for providing the *glpK*^{G184T} strain, and to Lin Chao and Camilla Ulla Rang for helping to acquire single-cell GFP images. This research is

supported by the NIH to TH (R01GM095903). RH was supported by NWO (VENI 680-47-419). TH additionally acknowledges the hospitality of the Institute for Theoretical Studies at ETH where some of this work was carried out.

REFERENCES

1. Monod J Recherches sur la croissance des cultures bactériennes, 210 p. (Hermann & cie, Paris, 1942).
2. Monod J The phenomenon of enzymatic adaptation - And its bearings on problems of genetics and cellular differentiation. Growth 11, 223–289 (1947).
3. Müller-Hill B The lac Operon : a short history of a genetic paradigm, ix, 207 p. (Walter de Gruyter, Berlin; New York, 1996).
4. Deutscher J, Francke C & Postma PW How phosphotransferase system-related protein phosphorylation regulates carbohydrate metabolism in bacteria. Microbiol Mol Biol Rev 70, 939–1031 (2006). [PubMed: 17158705]
5. Narang A & Pilyugin SS Bacterial gene regulation in diauxic and non-diauxic growth. J Theor Biol 244, 326–48 (2007). [PubMed: 16989865]
6. Loomis WF & Magasanik B Glucose-lactose diauxie in Escherichia coli. J Bacteriol 93, 1397–401 (1967). [PubMed: 5340309]
7. Inada T, Kimata K & Aiba H Mechanism responsible for glucose-lactose diauxie in Escherichia coli: challenge to the cAMP model. Genes Cells 1, 293–301 (1996). [PubMed: 9133663]
8. Lendenmann U, Snozzi M & Egli T Kinetics of the simultaneous utilization of sugar mixtures by Escherichia coli in continuous culture. Appl Environ Microbiol 62, 1493–9 (1996). [PubMed: 8633848]
9. Baidya TKN, Webb FC & Lilly MD The utilization of mixed sugars in continuous fermentation. I. Biotechnol. Bioeng. 9:195–204. *Biotechnol. Bioeng.***9**, 195–204 (1967).
10. Harte MJ & Webb FC Utilisation of mixed sugars in continuous fermentation. II. Biotechnol. Bioeng. 9, 205–221 (1967).
11. Harder W & Dijkhuizen L Strategies of mixed substrate utilization in microorganisms. Philos Trans R Soc Lond B Biol Sci 297, 459–80 (1982). [PubMed: 6180444]
12. Wanner U & Egli T Dynamics of microbial growth and cell composition in batch culture. FEMS Microbiol Rev 6, 19–43 (1990). [PubMed: 2186759]
13. Egli T, Lendenmann U & Snozzi M Kinetics of microbial growth with mixtures of carbon sources. Antonie Van Leeuwenhoek 63, 289–98 (1993). [PubMed: 8279825]
14. Hermsen R, Okano H, You C, Werner N & Hwa T A growth-rate composition formula for the growth of E.coli on co-utilized carbon substrates. Mol Syst Biol 11, 801 (2015). [PubMed: 25862745]
15. Lin EC Glycerol dissimilation and its regulation in bacteria. Annu Rev Microbiol 30, 535–78 (1976). [PubMed: 825019]
16. You C et al. Coordination of bacterial proteome with metabolism by cyclic AMP signalling. Nature 500, 301–6 (2013). [PubMed: 23925119]
17. Koch JP, Hayashi S & Lin EC The control of dissimilation of glycerol and L-alpha-glycerophosphate in Escherichia coli. J Biol Chem 239, 3106–8 (1964). [PubMed: 14217903]
18. Weissenborn DL, Wittekindt N & Larson TJ Structure and regulation of the glpFK operon encoding glycerol diffusion facilitator and glycerol kinase of Escherichia coli K-12. J Biol Chem 267, 6122–31 (1992). [PubMed: 1372899]
19. Zwaig N & Lin EC Feedback inhibition of glycerol kinase, a catabolic enzyme in Escherichia coli. Science 153, 755–7 (1966). [PubMed: 5328677]
20. Holtman CK, Pawlyk AC, Meadow ND & Pettigrew DW Reverse genetics of Escherichia coli glycerol kinase allosteric regulation and glucose control of glycerol utilization in vivo. J Bacteriol 183, 3336–44 (2001). [PubMed: 11344141]
21. Kochanowski K et al. Functioning of a metabolic flux sensor in Escherichia coli. Proc Natl Acad Sci U S A 110, 1130–5 (2013). [PubMed: 23277571]

22. Hui S et al. Quantitative proteomic analysis reveals a simple strategy of global resource allocation in bacteria. Mol Syst Biol 11, 784 (2015). [PubMed: 25678603]
23. Pettigrew DW, Liu WZ, Holmes C, Meadow ND & Roseman S A single amino acid change in Escherichia coli glycerol kinase abolishes glucose control of glycerol utilization in vivo. J Bacteriol 178, 2846–52 (1996). [PubMed: 8631672]
24. Kochanowski K et al. Few regulatory metabolites coordinate expression of central metabolic genes in Escherichia coli. Mol Syst Biol 13, 903 (2017). [PubMed: 28049137]
25. Applebee MK, Joyce AR, Conrad TM, Pettigrew DW & Palsson B Functional and metabolic effects of adaptive glycerol kinase (GLPK) mutants in Escherichia coli. J Biol Chem 286, 23150–9 (2011). [PubMed: 21550976]
26. Bettenbrock K et al. Correlation between growth rates, EIIACrr phosphorylation, and intracellular cyclic AMP levels in Escherichia coli K-12. J Bacteriol 189, 6891–900 (2007). [PubMed: 17675376]
27. Erickson DW et al. A global resource allocation strategy governs growth transition kinetics of Escherichia coli. Nature 551, 119–123 (2017). [PubMed: 29072300]
28. Keseler IM et al. The EcoCyc database: reflecting new knowledge about Escherichia coli K-12. Nucleic Acids Res 45, D543–D550 (2017). [PubMed: 27899573]
29. Mandelstam J The repression of constitutive beta-galactosidase in Escherichia coli by glucose and other carbon sources. Biochem J 82, 489–93 (1962). [PubMed: 14469207]
30. Müller S, Regensburger G & Steuer R Enzyme allocation problems in kinetic metabolic networks: optimal solutions are elementary flux modes. J Theor Biol 347, 182–90 (2014). [PubMed: 24295962]
31. Wortel MT, Peters H, Hulshof J, Teusink B & Bruggeman FJ Metabolic states with maximal specific rate carry flux through an elementary flux mode. FEBS J 281, 1547–55 (2014). [PubMed: 24460934]
32. Wang X, Xia K, Yang X & Tang C Growth strategy of microbes on mixed carbon sources. Nat Commun 10, 1279 (2019). [PubMed: 30894528]
33. Kumar R, Singh S & Singh OV Bioconversion of lignocellulosic biomass: biochemical and molecular perspectives. J Ind Microbiol Biotechnol 35, 377–91 (2008). [PubMed: 18338189]
34. Kim JH, Block DE & Mills DA Simultaneous consumption of pentose and hexose sugars: an optimal microbial phenotype for efficient fermentation of lignocellulosic biomass. Appl Microbiol Biotechnol 88, 1077–85 (2010). [PubMed: 20838789]
35. Vinuselvi P, Kim MK, Lee SK & Ghim CM Rewiring carbon catabolite repression for microbial cell factory. BMB Rep 45, 59–70 (2012). [PubMed: 22360882]
36. Soupene E et al. Physiological studies of Escherichia coli strain MG1655: growth defects and apparent cross-regulation of gene expression. J Bacteriol 185, 5611–26 (2003). [PubMed: 12949114]
37. Csonka LN, Ikeda TP, Fletcher SA & Kustu S The accumulation of glutamate is necessary for optimal growth of Salmonella typhimurium in media of high osmolality but not induction of the proU operon. J Bacteriol 176, 6324–33 (1994). [PubMed: 7929004]
38. Basan M et al. Inflating bacterial cells by increased protein synthesis. Mol Syst Biol 11, 836 (2015). [PubMed: 26519362]
39. Morrissey AT & Fraenkel DG Suppressor of phosphofructokinase mutations of Escherichia coli. J Bacteriol 112, 183–7 (1972). [PubMed: 4263401]
40. de Lorenzo V, Herrero M, Metzke M & Timmis KN An upstream XylR- and IHF-induced nucleoprotein complex regulates the sigma 54-dependent Pu promoter of TOL plasmid. EMBO J 10, 1159–67 (1991). [PubMed: 2022186]
41. Klumpp S, Zhang Z & Hwa T Growth rate-dependent global effects on gene expression in bacteria. Cell 139, 1366–75 (2009). [PubMed: 20064380]
42. Datsenko KA & Wanner BL One-step inactivation of chromosomal genes in Escherichia coli K-12 using PCR products. Proc Natl Acad Sci U S A 97, 6640–5 (2000). [PubMed: 10829079]
43. Kim M et al. Need-based activation of ammonium uptake in Escherichia coli. Mol Syst Biol 8, 616 (2012). [PubMed: 23010999]

44. McGowan MW, Artiss JD, Strandbergh DR & Zak B A peroxidase-coupled method for the colorimetric determination of serum triglycerides. Clin Chem 29, 538–42 (1983). [PubMed: 6825269]
45. Sévin DC & Sauer U Ubiquinone accumulation improves osmotic-stress tolerance in Escherichia coli. Nat Chem Biol 10, 266–72 (2014). [PubMed: 24509820]
46. Ogata H et al. KEGG: Kyoto Encyclopedia of Genes and Genomes. Nucleic Acids Res 27, 29–34 (1999). [PubMed: 9847135]
47. Schindelin J et al. Fiji: an open-source platform for biological-image analysis. Nat Methods 9, 676–82 (2012). [PubMed: 22743772]
48. Gornall AG, Bardawill CJ & David MM Determination of serum proteins by means of the biuret reaction. J Biol Chem 177, 751–66 (1949). [PubMed: 18110453]
49. Saier MH & Roseman S Sugar transport. Inducer exclusion and regulation of the melibiose, maltose, glycerol, and lactose transport systems by the phosphoenolpyruvate:sugar phosphotransferase system. J Biol Chem 251, 6606–15 (1976). [PubMed: 789370]
50. Sandermann H Jr. beta-D-Galactoside transport in Escherichia coli: substrate recognition. Eur J Biochem 80, 507–15 (1977). [PubMed: 336372]
51. Stock JB, Waygood EB, Meadow ND, Postma PW & Roseman S Sugar transport by the bacterial phosphotransferase system. The glucose receptors of the Salmonella typhimurium phosphotransferase system. J Biol Chem 257, 14543–52 (1982). [PubMed: 6292227]
52. Misset O, Blaauw M, Postma PW & Robillard GT Bacterial phosphoenolpyruvate-dependent phosphotransferase system. Mechanism of the transmembrane sugar translocation and phosphorylation. Biochemistry 22, 6163–70 (1983). [PubMed: 6362721]

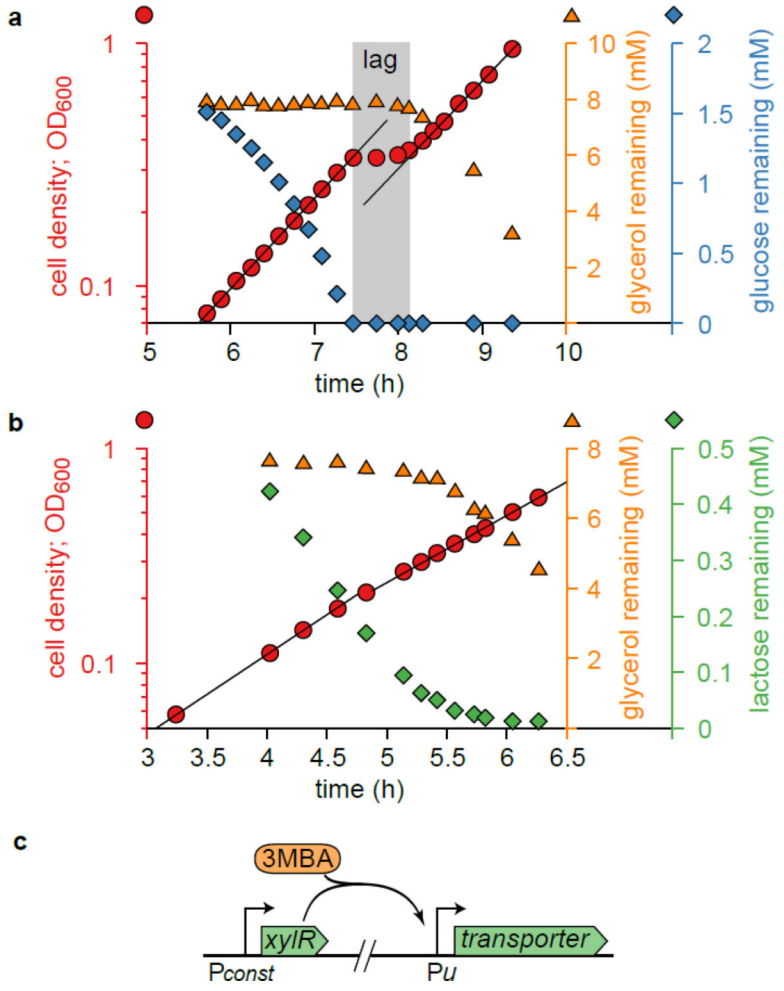

Figure 1. Diauxie and the titratable LacY or PtsG strains.

a. Diauxic growth of *E. coli* (NCM3722) grown on glycerol and glucose. The growth curve (OD_{600} vs. time, red circles) is shown together with measured concentrations of glycerol (orange triangles) and glucose (blue diamonds) remaining in the medium. Two growth phases—black lines are exponential fits—are separated by a lag time of about 40 min (gray shading). During the first growth phase, glucose is consumed, but glycerol is not. The lag phase starts when glucose is depleted; it ends when glycerol consumption begins.

b. As Panel a, but this time using lactose (green diamonds) instead of glucose. Despite the two distinct growth phases, no clear lag phase is observed. The slight consumption of glycerol (orange triangles) in the first phase is due to the low starting concentration of lactose (relative to the Michaelis constant of the lactose transporter), which is necessary for displaying diauxic growth; no glycerol is utilized at high enough lactose concentrations (see Extended Data 1g,h). Panel a,b clearly demonstrate *E. coli*'s preference for glucose and lactose over glycerol; yet, the growth curve of Fig. 1b does not exhibit the signature diauxic lag phase. This illustrates that the relation between hierarchical utilization and diauxic growth is not one-to-one and depends on the specifics of the system.

c. Illustration of the genetic constructs used to titrate the expression of substrate uptake (transporter) enzymes by varying the amount of inducer 3MBA in the medium. See Supplementary Figure 1a–c and Supplementary Table 1 for details.

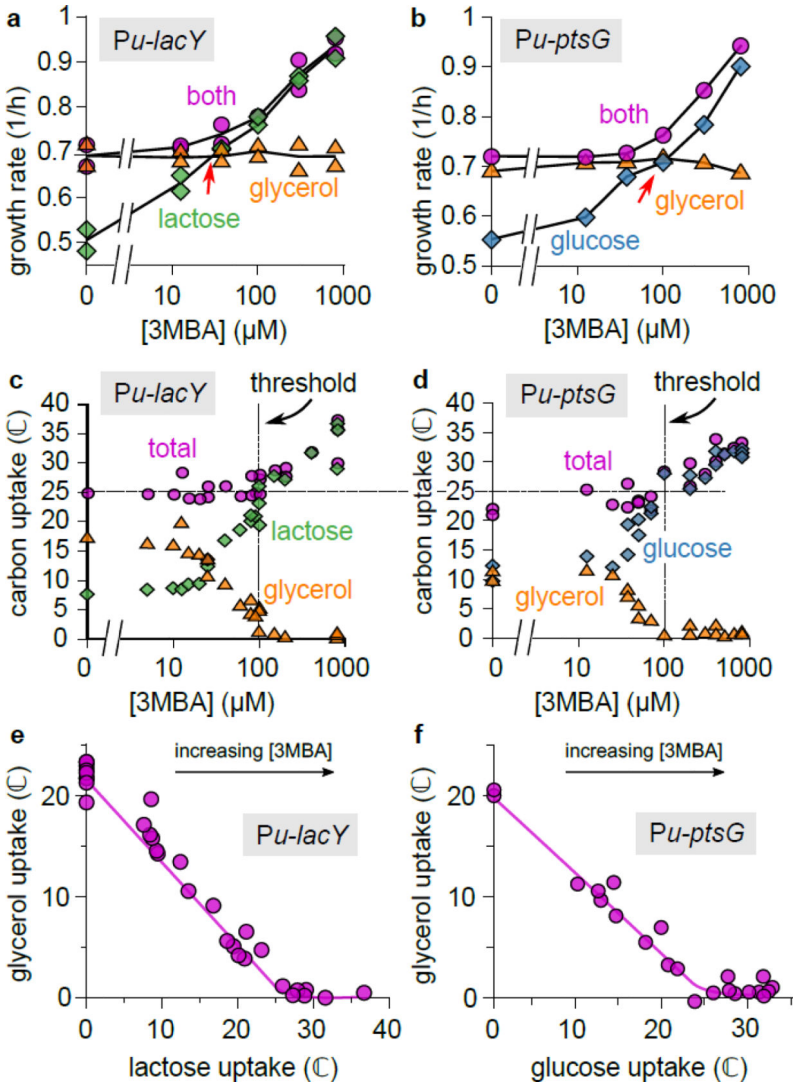

Figure 2. Uptake fluxes reveal hierarchical and simultaneous utilization regimes.

a. Growth rates for the titratable LacY strain (NQ917), grown on lactose, glycerol, or both, at various 3MBA concentrations. To demonstrate the reproducibility of the data, results from two independent experiments are shown for each condition.

b. As Panel a, but for the titratable PtsG strain (NQ1243), with glucose instead of lactose. Other substrate combinations show similar patterns; see Extended Data 2.

c. Lactose and glycerol uptake (in ℂ = mM of carbon atoms per OD_{600} per hour) by the titratable LacY strain (NQ917) at various 3MBA concentrations. If lactose uptake is below a threshold of ≈ 25 ℂ (horizontal dashed line), glycerol is consumed, too. In this regime (left of the dashed vertical line), the total carbon uptake stays approximately constant despite a threefold change in lactose uptake. Also see Supplementary Figure 2.

d. As Panel c, but using the titratable PtsG strain (NQ1243) and glucose instead of lactose. A strikingly similar threshold of ≈ 25 ℂ is found for the onset of glycerol utilization.

e. Plotting glycerol uptake versus lactose uptake (the “flux relation”) of the titratable LacY strain reveals a threshold-linear relation. (The solid line is a guide to the eye.)

f. As Panel e, but for the titratable PtsG strain with glucose instead of lactose. The flux relation is remarkably similar to that of Panel e.

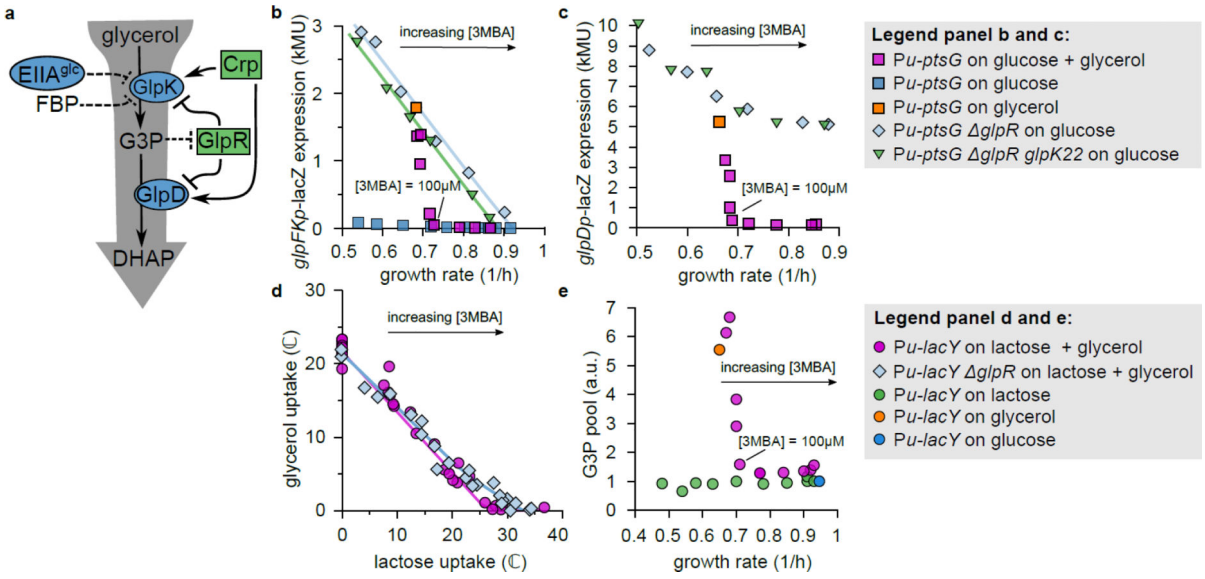

Figure 3. Glycerol uptake involves derepression of glycerol catabolic genes.

a. Known regulation of glycerol uptake under aerobic conditions. Blue ovals represent enzymes, green rectangles transcriptional regulators. Dashed lines indicate allosteric inhibition[18,19,49]. See Supplementary Figure 4 for more details.

b. LacZ reporter expression from the *glpFK* promoter versus growth rate in titratable PtsG strains (HE305 and mutants thereof) with varying 3MBA levels. In the presence of glucose + glycerol (purple squares) expression fell abruptly if the growth rate exceeded that on glycerol alone (orange square). In contrast, in the *ΔglpR* or *ΔglpR glpK22* background (pale blue diamonds and green triangles) the expression followed a straight line (a "C-line"[16]). (Regression lines are shown. *ΔglpR* strain: $R^2_{adj} = 0.98$, $n = 6$ conditions, $t = 17.6$, df = 4, two-sided $p = 6.1 \times 10^{-5}$. *ΔglpR glpK22* strain: $R^2_{adj} = 0.99$, $n = 6$ conditions, $t = 46.0$, df = 4, two − sided $p = 1.3 \times 10^{-6}$.) Little expression was observed on glucose alone (blue squares).

c. As Panel b, except that expression from the *glpD* promoter was measured (strain HE397 and mutants thereof). Again, in the presence of glucose + glycerol (purple squares) expression turned off abruptly if the growth rate exceeded that on glycerol alone (orange square). However, reporter expression in the *ΔglpR* or *ΔglpR glpK22* background (pale blue diamonds and green triangles) responded more moderately and displayed a high background level.

d. Comparison between the flux relations of the *ΔglpR* strain (NQ958) and the *glpR*$^+$ strain (NQ917) in the titratable LacY background. The threshold-linear shape is less prominent in *ΔglpR* (blue diamonds) than in *glpR*$^+$ (purple circles). (Solid lines are guides to the eye.)

e. Intracellular G3P pool versus growth rate in the titratable LacY strain (NQ917) grown on lactose + glycerol with various 3MBA concentrations (purple circles), lactose alone with various 3MBA concentrations (green circles), glycerol alone without 3MBA (orange circle), and glucose alone without 3MBA (blue circle). The measurements for each mass spectrometry run were normalized by the result for growth on lactose alone with [3MBA] = 800 mM. In the presence of lactose + glycerol, the G3P pool abruptly drops if the growth rate exceeds that on glycerol alone.

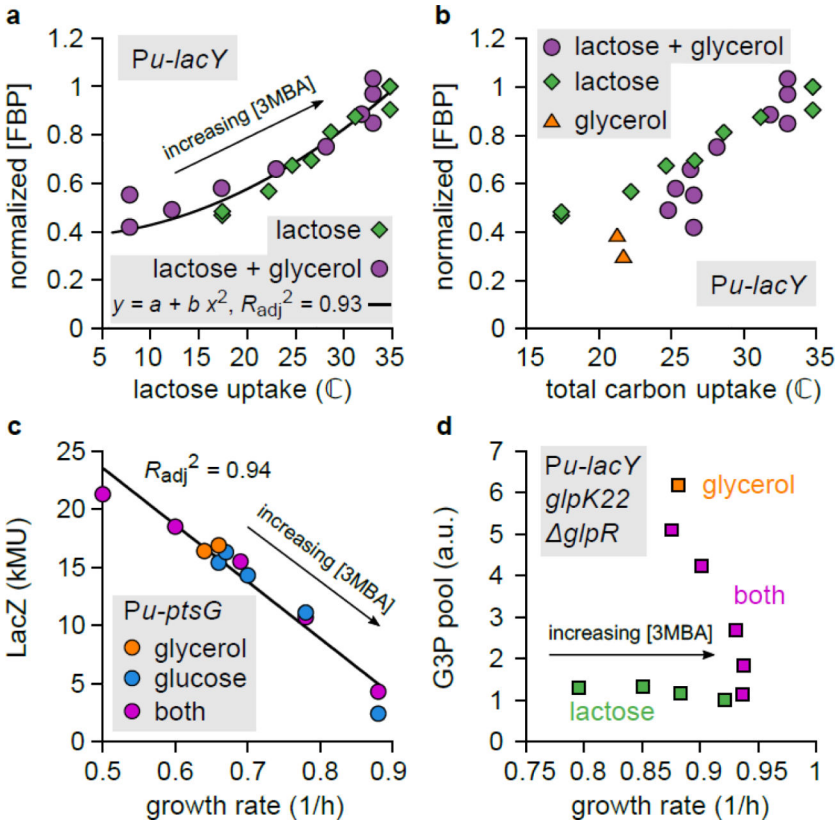

Figure 4. Glycerol uptake is regulated by two flux sensors: FBP and cAMP–Crp.

a. Intracellular FBP pool in the titratable LacY strain (NQ917) grown on lactose + glycerol or lactose alone, plotted against the lactose uptake flux. The results of each run of mass spectrometry were normalized by the result on lactose alone with [3MBA] = 800 mM. The black line is a quadratic fit ($y = a + b\,x^2$; $R^2_{\text{adj}} = 0.93$, $n = 22$ experimental conditions, $t = 16.7$, df = 20, two-sided $p = 3 \times 10^{-13}$). The FBP pool can be considered a function of the lactose uptake flux alone.

b. As Panel a, but now with *total* carbon flux on the horizontal axis. The FBP pool cannot be considered a function of the total carbon-uptake flux because the three datasets do not collapse.

c. LacZ expression levels from the native *lac* promoter in the titratable PtsG strain (NQ1243) grown on glucose alone, glycerol alone, or both, with various 3MBA concentrations, plotted against the growth rate. Because IPTG (1 mM) was added to remove repression by LacI, expression is a proxy for cAMP–Crp activity. The black line is a linear regression ($R^2_{\text{adj}} = 0.94$, $n = 12$ experimental conditions, $t = 13$, df = 10, two-sided $p = 1.3 \times 10^{-7}$). The data collapse on a single trend line (a "C-line"[16]), demonstrating that activation by cAMP–Crp can be considered a function of the growth rate or the total carbon-uptake flux.

d. G3P pool in the titratable LacY strain with *ΔglpR glpK22* mutations (NQ1187). When grown on lactose + glycerol with varying amounts of 3MBA, the G3P pool responds sharply to changes in the growth rate. Because the *ΔglpR glpK22* mutations remove GlpR repression

and allosteric inhibition by FBP, this demonstrates that cAMP-Crp signaling affects the G3P level.

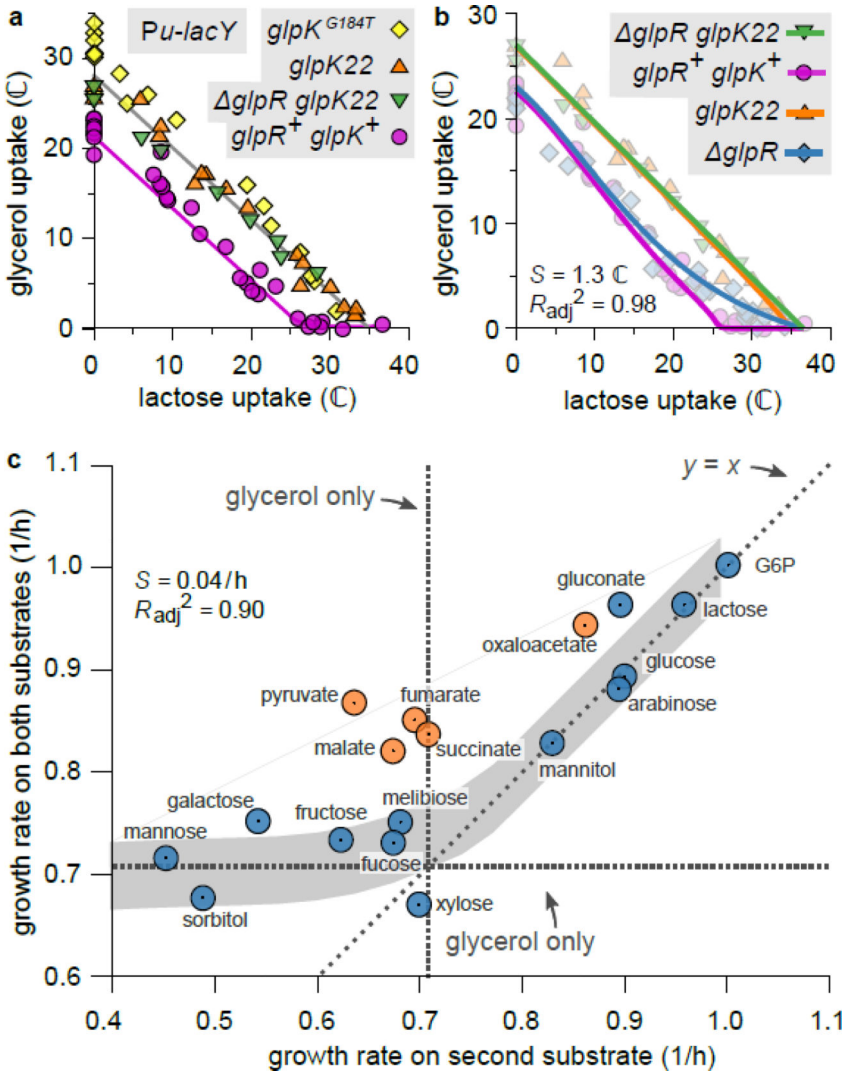

Figure 5. Analysis, modeling and predictions.

a. Comparison between the flux relations of strains harboring the *glpK*^{G184T} mutation (NQ959), the *glpK22* mutation (NQ1186), or the *ΔglpR glpK*22 double mutation (NQ1187), and the wild-type *glpK* (NQ917, *glpR*$^+$ *glpK*$^+$) in the titratable LacY background. In the mutant strains the threshold-linear shape is lost, and the flux relation is nearly linear. (Linear regression for *glpK*^{G184T}:$R^2_{adj} = 0.97$, $n = 18$ conditions, $t = 22.6$, df = 16, $p = 1 \times 10^{-13}$. For *glpK22*:$R^2_{adj} = 0.98$, $n = 18$, $t = 29.7$, df = 16, conditions, $p = 2 \times 10^{-15}$. For *ΔglpR glpK*22: $R^2_{adj} = 0.99$, $n = 8$ conditions, $t = 27.8$, df = 6, $p = 1 \times 10^{-7}$.) Lines are guides to the eye.

b. Model fits of the flux relations for various strains (solid lines) together with the corresponding measurements (background symbols). A single set of parameter values (given in Supplementary Table 3) fits the data of all strains ($R^2_{adj} = 0.98$, standard error of the regression $S = 1.3$ ℂ, $n = 84$ experimental conditions). The same model and parameters also reproduce G3P measurements and expression data (see Extended Data 6).

c. Growth rate of WT cells (NCM3722) in the presence of glycerol plus a "second" substrate, versus growth rate on the second substrate only, for many second substrates. Plotted is the mean of $n = 2$ to 4 independent replicates (see Source Data). Horizontal and vertical dashed lines indicate the growth rate on glycerol only. If the second carbon substrate is processed by upper glycolysis (blue circles; errors are of the order of the symbol size), the model predicts hierarchical utilization (gray band; width is estimated SE of the prediction, assuming an independent error in the predicted uptake of each substrate of $S = 1.3$ ℂ, as in Panel b; fit quality: $R^2_{\text{adj}} = 0.90$, $S = 0.04$ /h, $n = 13$ independent measurements). Therefore, the growth rate on both substrates is approximately the larger of the two single-substrate growth rates. In contrast, if the second substrate is gluconeogenic (orange circles), the growth rate on both substrates is larger than on either substrate alone (two-sided paired t-test, $n = 5$ cases, $t = 9.26$, df = 4, $p = 8 \times 10^{-4}$), reflecting simultaneous utilization. A similar trend is seen if xylose or fucose are used instead of glycerol (Extended Data 7b,c).